Cellular/Molecular

Acute Complement Inhibition Potentiates Neurorehabilitation and Enhances tPA-Mediated Neuroprotection

Ali Alawieh,[1,2] Meredith Andersen,[1] DeAnna L. Adkins,[3,4,5] and Stephen Tomlinson[1,5]

[1]Department of Microbiology and Immunology, [2]Medical Scientist Training Program, College of Medicine, [3]Department of Neurosciences, [4]College of Health Professions, Medical University of South Carolina, Charleston, South Carolina 29425, and [5]Ralph Johnson VA Medical Center, Charleston, South Carolina 29425

Because complement activation in the subacute or chronic phase after stroke was recently shown to stimulate neural plasticity, we investigated how complement activation and complement inhibition in the acute phase after murine stroke interacts with subsequent rehabilitation therapy to modulate neuroinflammation and neural remodeling. We additionally investigated how complement and complement inhibition interacts with tissue plasminogen activator (tPA), the other standard of care therapy for stroke, and a U.S. Food and Drug Administration preclinical requirement for translation of an experimental stroke therapy. CR2fH, an injury site-targeted inhibitor of the alternative complement pathway, significantly reduced infarct volume, hemorrhagic transformation, and mortality and significantly improved long-term motor and cognitive performance when administered 1.5 or 24 h after middle cerebral artery occlusion. CR2fH interrupted a poststroke inflammatory process and significantly reduced inflammatory cytokine release, microglial activation, and astrocytosis. Rehabilitation alone showed mild anti-inflammatory effects, including reduced complement activation, but only improved cognitive recovery. CR2fH combined with rehabilitation significantly potentiated cognitive and motor recovery compared with either intervention alone and was associated with higher growth factor release and enhanced rehabilitation-induced neuroblast migration and axonal remodeling. Similar outcomes were seen in adult, aged, and female mice. Using a microembolic model, CR2fH administered in combination with acute tPA therapy improved overall survival and enhanced the neuroprotective effects of tPA, extending the treatment window for tPA therapy. A human counterpart of CR2fH has been shown to be safe and nonimmunogenic in humans and we have demonstrated robust deposition of C3d, the CR2fH targeting epitope, in ischemic human brains after stroke.

Key words: complement; rehabilitation; thrombolysis

Significance Statement

Complement inhibition is a potential therapeutic approach for stroke, but it is not known how complement inhibition would interact with current standards of care. We show that, after murine ischemic stroke, rehabilitation alone induced mild anti-inflammatory effects and improved cognitive, but not motor recovery. However, brain-targeted and specific inhibition of the alternative complement pathway, when combined with rehabilitation, significantly potentiated cognitive and motor recovery compared with either intervention alone via mechanisms involving neuroregeneration and enhanced brain remodeling. Further, inhibiting the alternative pathway of complement significantly enhanced the neuroprotective effects of thrombolytic therapy and markedly expanded the therapeutic window for thrombolytic therapy.

Introduction

Stroke induces a time-sensitive window of heightened neural plasticity in which the brain's ability to form new neurons or reorganize existing neural connections is increased (Murphy and Corbett, 2009). Neurorehabilitation treatments delivered during this window result in enhanced recovery and greater neural plasticity compared with no rehabilitation or rehabilitation delivered

Received Jan. 17, 2018; revised May 25, 2018; accepted May 31, 2018.

Author contributions: A.A. wrote the first draft of the paper; D.L.A. and S.T. edited the paper; A.A., D.L.A., and S.T. designed research; A.A. and M.A. performed research; A.A., M.A., D.L.A., and S.T. analyzed data; S.T. wrote the paper.

This work was supported by the National Institutes of Health (Grants R21NS097653, 1P20GM109040, U54-GM10491, and P2CHD086844), the Department of Veterans Affairs (Merit Awards 1I01RX001141, 1BX001218, and 21RX002363), and the American Heart Association (Predoctoral Fellowship 15PRE25250009 to A.A.). We thank the Carroll A. Campbell, Jr. Neuropathology Laboratory (Drs. L. Granholm and K. Bharani) for providing human brain samples; the MUSC Cell and Molecular Imaging Core (funded by NIH Grants P30 CA138313 and S10 OD018113) and the Center for Oral Health Research (funded by National Institute of General Medical Sciences–NIH Award P30GM103331) for tissue imaging equipment; and the Center for Biomedical Imaging (Drs. M. Falangola, X. Nie, and R. Deardorff) for assistance with small animal imaging.

S.T. is an inventor on a licensed patent for CR2-targeted complement inhibitors. The remaining authors declare no competing financial interests.

Correspondence should be addressed to Dr. Stephen Tomlinson, Department of Microbiology and Immunology, Medical University of South Carolina, 173 Ashley Avenue, BSB 204, Charleston, SC 29425. E-mail: tomlinss@musc.edu.

DOI:10.1523/JNEUROSCI.0111-18.2018

 0270-6474/18/386527-19$15.00/0

outside of this period (Jones and Adkins, 2015; Carmichael et al., 2017). Therefore, a treatment that can both limit early neurodegenerative events and enhance the proregenerative environment after stroke may limit tissue loss, reduce overall deficits, and enhance the efficacy of rehabilitation-induced recovery and neural repair.

Poststroke inflammation is implicated in promoting secondary injury leading to increased damage and inhibited recovery (Alawieh et al., 2015a). The complement system is one component of inflammation implicated in early neurodegenerative events after stroke (Alawieh et al., 2015b) and its ability to activate multiple inflammatory pathways has made complement an attractive therapeutic target in neurodegenerative and neuroinflammatory diseases (Brennan et al., 2016). Inhibition of complement after stroke has been shown to reduce infarct volume, functional deficits, thrombosis, endothelial activation, and leukocyte migration in the acute phase (Alawieh et al., 2015a). However, complement activation products are also involved in poststroke recovery and regeneration (Alawieh et al., 2015a; Moran et al., 2017; Stokowska et al., 2017) and total blockade of complement activation in mice by deficiency or inhibition is not protective past the acute phase (Alawieh et al., 2015b). In this context, we demonstrated previously that CR2fH, an inhibitor specific for the alternative complement pathway (ACP), provided both acute and subacute (7 d) protection, whereas an inhibitor of all complement pathways (CR2Crry) did not provide neuroprotection past the acute phase (Alawieh et al., 2015b). These complement inhibitors are fusion proteins constructed by fusing a complement inhibitor (fH or Crry) to a fragment of complement receptor 2 (CR2) that targets the complement inhibitor to sites of C3d deposition, a complement activation product covalently bound at sites of complement activation. This targeting approach improves bioavailability and significantly improves the efficacy of complement inhibition without the immunosuppressive effects of systemic complement inhibition (Atkinson et al., 2005).

We investigated the interaction among complement, complement inhibition, and rehabilitation-induced neuroplasticity and neuroregeneration and how these interactions affect poststroke outcomes. Further, because the Stroke Treatment Academic Industry Roundtable (STAIR) recommendations and U.S. Food and Drug Administration (FDA) requirements state that any new investigational agent for stroke must be tested in combination with tPA, the only approved pharmacologic standard of care for stroke, we additionally investigated complement inhibition in the context of tPA therapy.

Materials and Methods

Stroke models. To model transient middle cerebral artery occlusion (MCAO), adult C57BL/6 (males and females) mice were obtained from The Jackson Laboratory and allowed 1 week of acclimation before use. $fB^{-/-}$ mice on C57BL/6 background were bred onsite. Adult animals were 12 weeks old and aged animals were 14 months old at the time of stroke surgeries. After anesthesia using ketamine (80–100 mg/kg, i.p.) and xylazine (i.p., 10 mg/kg), transient MCAO was induced using a blunted 5–0 nylon suture inserted through the internal carotid artery to the origin of the MCA as described previously (Alawieh et al., 2015b). The suture was withdrawn after 60 min, allowing for reperfusion. Laser Doppler flow monitoring (moorVMS-LDF1 device; Moor Instruments) was used to assess uniform induction of ischemia across animals. Animals with <80% reduction in ipsilateral cerebral blood flow compared with presurgical baseline were excluded from study. There were no significant difference in weight, heart rate, respiratory rate, or extent of reduction of blood flow between all treatment groups ($p > 0.05$). After surgery and during recovery from anesthesia, temperature was maintained at ~37°C as assessed by rectal probe and animals were housed in a temperature- and humidity-controlled chamber until recovery from anesthesia and return to regular housing. No significant difference of intraprocedural and periprocedural temperature was noted between the different groups. CR2fH (16 mg/kg) was administered intravenously via tail vein injections at designated time points after ischemia. All animal studies were approved by the Institutional Animal Care and Use Committee (IACUC) at the Medical University of South Carolina. Animals are allowed *ad libitum* access to water and food during the entire experiment. DietGel Recovery food (ClearH2O) was provided to the animals during the first 2 d of poststroke recovery. Throughout the study, a total of 118 animals received vehicle treatment (14 cohorts) and 89 animals received CR2fH 90 min after ischemia (14 cohorts).

Microembolic stroke was performed as described previously (Alawieh et al., 2016). In brief, the overall surgical procedure was performed similar to the MCAO procedure, but instead of insertion of the 6-0 nylon filament, freshly prepared emboli at concentrations of 1×10^8 emboli/ml (0.1 ml total bolus) at a size range of 1.9–7.7 μm in diameter were injected through a polyethylene catheter with inner diameter of 0.02 mm (Braintree Scientific) placed at the origin of the MCA. After emboli administration, tissue plasminogen activator Cathflo Activase (Alteplase; Genentech) was injected as an intravenous bolus (8 mg/kg) via tail vein followed by CR2fH 2 h after emboli administration.

Recombinant proteins. The recombinant complement inhibitor CR2fH used in this study was constructed, expressed, purified, and subjected to quality control for complement inhibitory activity using chicken red blood cell lysis assay and zymosan assay as described previously (Huang et al., 2008; Alawieh et al., 2015b).

Brain hemoglobin content. Hemoglobin content in the brain was measured using Drabkin's reagent (D5941; Sigma-Aldrich) according to the manufacturer's recommendations. After intracardiac perfusion using ice-cold PBS, the entire ipsilateral hemisphere was homogenized in NP-40 lysis buffer (Invitrogen) and then centrifuged at 13,000 rpm for 30 min. The supernatant was incubated with Drabkin's reagent for 15 min at room temperature and absorbance was read at 540 nm. Cyanmethemoglobin was used at standard concentrations to construct a calibration curve.

C3a and C5a measurement. C3a and C5a levels were measured by ELISA on brain homogenates prepared from the ipsilateral hemisphere after MCAO using mouse C3a and C5a ELISA kits (Kamiya Biomedical) according to the manufacturer's recommendations. Brain tissue was homogenized using NP-40 lysis buffer (Invitrogen) supplemented with PMSF (Sigma-Aldrich), protease inhibitor mixture (Sigma-Aldrich), and Nafamostat mesylate (FUT-175; Sigma-Aldrich).

Rehabilitation paradigm. As a preclinical model of poststroke rehabilitation, we used a combined setup of motor and cognitive rehabilitation starting 48 h after ischemia. Animals in the rehabilitation group were housed in larger cages with toys, ladders, running wheels, and pipes that allowed motor and cognitive engagement of the animals. These items were rearranged and changed twice per week. Pieces of vermicelli pasta (2.4 cm in length) were added to the rehabilitation cages daily to stimulate forearm handling. Animals in the non-rehabilitation groups were housed in regular cages without additional enrichment and received short pieces of pasta daily (0.4 cm in length). At different time points after starting rehabilitation therapy, animals in the rehabilitation groups were recorded for 15 min sessions to assess toy interactions.

T2-weighted and diffusion MRI. MRI scans were acquired on days 4 and 14 after stroke using a 7T/30 Bruker Biospec animal scanner. T2-weighted images were used to quantify lesion size by measuring the volume of T2 hyperintensity from 15 2-mm-thick sections. Diffusion imaging was performed using a 2 shot spin-echo echo planar diffusion sequence with 30 diffusion-encoding directions and 3 b values: 0, 1000, and 2000 s/mm^2. Other imaging parameters included repetition time: 3750 ms, echo time: 3750/32.5 ms, field of view: 30 mm × 30 mm, matrix: 128 × 128, and number of excitations: 2. A total of 15 axial slices with no gap were collected at a thickness of 2 mm. Diffusion and diffusional kurtosis tensors were calculated using diffusional kurtosis estimator (Tabesh et al., 2011). Regions of interest (ROIs) were drawn over three

locations in the ipsilateral (stroke) hemisphere: basal ganglia, ipsilesional cortex, and ipsilesional hippocampus. Symmetric ROIs were drawn in the contralesional hemisphere and the ratio of ipsilateral-to-contralateral mean diffusivity (MD) and mean kurtosis (MK) were computed at each ROI (basal ganglia, cortex, and hippocampus). MD and MK reflect the apparent diffusion and kurtosis coefficients averaged over all directions.

Infarct volume and lesion size assessment. Lesion size, including scarring, was estimated using Nissl staining of serial brain sections. Brains were harvested 1 and 15 d after stroke after cardiac perfusion with ice-cold PBS and 4% paraformaldehyde (PFA). Brains were then cryoprotected using 30% sucrose in PFA and then cut into 40-μm-thick coronal sections. Serial sections 200 μm apart were mounted and stained using cresyl violet as described previously (Türeyen et al., 2004). Slides were then imaged using Olympus BX61 light microscope with Visiopharm image acquisition and analysis software. To quantify and locate lesions anatomically, Nissl-stained images were aligned to Paxinos' brain atlas and lesion location (infarct and astrogliosis) was mapped to the atlas sections. Images from multiple animals of the same group were superimposed to generate heat maps using MATLAB 2015 to show the frequency of involvement of different brain regions in injury. After lesion mapping, 3D reconstruction of lesions and brains was conducted on Amira version 6.2 software (FEI) and volume was computed in cubic millimeters.

Neurological deficit scoring and assessment of motor recovery. To assess functional recovery, animals were scored daily by two blinded observers using the neurological deficit score described previously (Elvington et al., 2012). Animals received a score of 0 for normal motor function, 1 for torso and contralateral forelimb flexion when lifted by tail, 2 for contralateral circling when held by tail on flat surface, 3 for contralateral leaning when at rest, and 4 for no spontaneous motor activity. Forelimb asymmetry was measured using corner test as described previously (Zhang et al., 2002). Laterality was measured at baseline and after surgery. The normalized laterality index was calculated as follows: [(laterality at time t) + 2]/[(baseline laterality) + 2)]. Open-field locomotor testing was performed as described previously (Elvington et al., 2012). Animals were videotaped and videos were analyzed using the Autotyping toolbox (University of Pennsylvania). Total distance moved and the duration of movement were computed to assess ambulation and time spent at the center versus periphery was used to assess differences in anxiety levels. The pasta-handling task was performed by training all mice to handle 2.4-cm-long pieces of vermicelli in a transparent chamber and was video-recorded as described previously (Tennant et al., 2010). Videos were quantified for the time to eat each piece, the percentage of total handling time spent with the piece of pasta held only by the contralateral hand (unilateral handling), and the total number of adjustments per piece.

Assessment of cognitive recovery. To assess the impact of the different interventions on spatial learning and memory retention, both passive avoidance and Barnes maze tasks were used. Avoidance learning was assessed using an automated passive avoidance apparatus (Coulbourn Instruments) with automated sensing and shock systems (GraphicState 4; Coulbourn Instruments). Animals were trained to associate a shock with the dark chamber of a double chamber box and were tested at baseline and after stroke for retention of avoidance memory using the time to enter the dark chamber as described previously (Alawieh et al., 2015b). Barnes maze was used to assess spatial learning after stroke using a previously described protocol (Patil et al., 2009). Animals were trained for 2 trials a day for 5 d starting day 8 after stoke while being video-recorded. Videos were then analyzed automatically using the Autotyping toolbox (University of Pennsylvania) to compute the total path length and the number of error pokes before animals reach the escape box.

Principal component analysis (PCA). To globally assess the effect of different interventions on motor and cognitive recovery after stroke, performance on the different motor and cognitive tasks acutely (day 1), subacutely (day 7), and long-term (day 15) were used as inputs to compute the PCs that can explain the variance in the data and classify the groups. The two or three main PCs that explained >90% of the variance across all measures were used to plot individual data points for each animal, including both stroke and sham animals. Similar PCA analyses were performed on all motor and cognitive measures and then on motor and cognitive measures individually. To aid in visualization, a vector originating from the center of the sham group cluster pointing to the center of the vehicle group cluster reflects the direction of increased deficits/impairment.

Immunohistochemical (IHC) staining. IHC staining was performed on 40 μm sections prepared as described above. Free-floating sections were incubated with 3% H_2O_2 followed by 0.1% Triton X-100 in PBS, blocked in 5% horse serum, and incubated with primary antibodies overnight. Sections were then washed, incubated with HRP-conjugated secondary antibodies, and developed using DAB (ImmPress DAB; Vector Laboratories). Sections were mounted on slides, counterstained with hematoxylin, and imaged using an Olympus BX61 light microscope with Visiopharm image acquisition and analysis software. Antibodies used in IHC studies were anti-Doublecortin (Dcx) (Abcam), anti-GAP43 (Abcam), anti-MAP2 (Abcam), and anti-PSD95 (Abcam) with HRP-anti-rabbit secondary (Vector Laboratories).

Immunofluorescence staining and imaging. A similar approach was used to stain 40 μm sections as outlined above. Primary antibodies used for these experiments were against murine antigens and include anti-C3d (goat Ab; R&D Systems), anti-Iba1 (goat Ab; Abcam), anti-Mac2 (goat Ab; R&D Systems), anti-GFAP (rat Ab; Abcam), and anti-GAP43 (rabbit Ab; Abcam). Directly conjugated antibodies used were as follows: anti-human C3/C3d-FITC (MP Biomedicals) and anti-IgM-FITC (Millipore). Secondary antibodies used were as follows: donkey anti-goat-Alexa Fluor 488 nm and 555 nm, donkey anti-rabbit-Alexa Fluor 488 nm, 555 nm and 647 nm, donkey anti-rat Alexa Fluor 488 nm and 555 nm. DAPI (Vector Laboratories) was used as nuclear stain. NeuroTrace (647 nm; Invitrogen) was used to label neurons. Slides were mounted with Vectashield mounting medium (±DAPI) before microscopy. Epifluorescence microscopy was used to image full-brain sections using an Olympus BX61 light microscope with Visiopharm image acquisition and analysis software. Counts of number of cells per field were obtained from randomly assigned fields from the perilesional tissue using a motorized stage apparatus and analyzed using ImageJ. Intensity-based analysis was automatically computed using MATLAB by normalizing the intensity of signal to the area of tissue displayed per random field. Super-resolution imaging was performed using a Zeiss LSM 880 confocal microscope and Airy Scan was used for high-resolution fields. Fields were imaged using 40× water objective. High-resolution microglial fields were imaged at the 63× oil objective. 3D rendering was performed using ZEN-blue and ZEN-black software (Zeiss) and image analysis was performed using both ZEN (Zeiss) and ImageJ software.

Nanostring gene expression analysis. High-throughput gene expression analysis of immunology-related genes was performed using the Nanostring Mouse Immunology Codeset (Nanostring Technologies) that includes 561 immunology-related genes. Ipsilateral hemispheres were extracted from animals perfused 5 d after MCAO and treated with vehicle, rehabilitation, CR2fH or combination therapy. RNA was extracted using RNeasy Lipid Tissue kit (Qiagen). Analysis was performed using the Nanostring nCounter Analysis System (Nanostring Technologies). Each reaction contained 250 ng of total RNA in a 5 μl aliquot plus reporter and capture probes and six pairs of positive control and eight pairs of negative control probes. Analysis and normalization of the raw Nanostring data was conducted using nSolver Analysis software version 1.1 (Nanostring Technologies). Raw counts were normalized to levels of reference gene as described previously. Genes were considered differentially regulated for $p < 0.01$ on Student's t test performed on replicate data ($n = 5$) as described previously (Geiss et al., 2008). Clustergrams and PCA were performed in MATLAB 2013 and analysis of gene ontology (GO) biological processes was performed using PANTHER (Mi et al., 2016).

Western blot. After cardiac perfusion with ice-cold PBS, ipsilateral hemispheres were extracted and homogenized in NP-40 lysis buffer (Invitrogen) containing 1 mM PMSF (Sigma-Aldrich), 92.6 μm FUT175 (Sigma-Aldrich), and 5 μl of protease inhibitor mixture (Sigma-Aldrich). Protein concentrations were determined using BCA protein assay kit (Thermo Scientific). Antibodies against mouse TNF-α (Ab-

cam), GAPDH (Abcam), BDNF (Abcam), and β-actin (Santa Cruz Biotechnology) were used to assess proteins levels by Western blotting of 25 μg of total protein, with SDS-PAGE run under reducing conditions, and detected with HRP-conjugated secondary antibodies (Vector Laboratories). Signal densities were calculated relative to β-actin or GAPDH using Quantity One anlaysis software (Bio-Rad).

Human brain staining. Immunostaining for IgM and C3d deposition in the ischemic brain was performed on fresh-frozen sections of postmortem human brain. Human postmortem brain tissue was obtained from the Carroll A. Campbell, Jr. Neuropathology Laboratory at the Medical University of South Carolina from three patients who died from acute stroke (24–72 h). Frozen sections were cut at 6 μm thickness and stained using anti-IgM and anti-C3d. Intensity of binding was quantified automatically as described above. All procedures involving human brain tissue were approved by the institutional review board at the Medical University of South Carolina through an exempt application.

Experimental design and statistical analysis. The overall experimental design of the studies included pretraining animals on behavioral tasks followed by MCAO surgeries and random allocation to different treatment groups. Animals were killed at predefined endpoints for each experiment. Animals were randomly assigned to the different treatment groups (vehicle, vehicle + rehabilitation, CR2fH, and CR2fH + rehabilitation) before the acclimation on behavior tasks before the surgeries. Laboratory personnel involved in surgeries, administration of treatment, testing, and scoring animals were blinded to the group allocations for the duration of the study. To ensure that testing was performed in a blinded setting, animals assigned to rehabilitation cages were placed in regular cages before testing by laboratory personnel. Reasons for animal exclusion from studies included the following: mortality during surgery, before surgery, or before administration of treatment (~7% of animals) or failure to successful accomplish training on behavioral testing before surgery (2% of all animals). Animals dying within 2 d of stroke in studies involving rehabilitation were excluded to limit the impact of early mortality on these data and because randomization to rehabilitation occured 48 h after MCAO. Endpoints were predefined for each experiment by a time after reperfusion of 24 h (acute studies), 5 d (Nanostring analysis), and 15 d (long-term studies). Humane endpoints were determined by institutional guidelines in accordance with IACUC recommendations. For long-term studies, analysis was performed with a last observation carried forward paradigm in the event of mortality beyond 2 d of reperfusion. Neurological deficit scoring and analysis of pasta-handling task were independently performed by two blinded observers. Behavioral assessments (open field, passive avoidance, and Barnes maze) were analyzed using automated devices and video analysis tools. Individual animals (not fields in histological studies) were considered a unit for statistical analyses. Sample size determination was performed using G*Power 3.1 (Heinrich-Heine-Universität, Düsseldorf, Germany). Effect size for different behavioral analyses was determined based on prior studies with CR2fH and calculations were made based on the following criteria: power of 80% and a significance level <0.05 (corrected for multiple comparisons wherever appropriate). For histological analyses, an anticipated 1.5–2 times higher neuronal density is expected in treated animals compared with vehicle, so a group size of 6 is required to achieve an 84% power with a significance level <0.05 corrected for multiple comparisons.

Statistical analyses were performed using GraphPad Prism version 6.0 software. Parametric testing was used unless otherwise specified. Group analyses were performed using one-way ANOVA (or two-way ANOVA for multiple time points) followed by multiple-comparisons analyses using Bonferroni's test or repeated-measures ANOVA for matched data. p-values <0.05 were considered significant. Student's t test (two-tailed) was used to compare two groups. Pearson correlation coefficients were used to compute correlations. Proportion statistics was compared used χ^2 test. Brown–Forsythe test was used to assess for homogeneity of variance when parametric testing was used. PCA analysis was performed as described above using MATLAB.

Results

Inhibition of the ACP limits acute infarct volume and hemorrhagic transformation

Hemorrhagic transformation is a fatal complication of ischemic stroke. Complement anaphylatoxins (C3a and C5a) are involved in endothelial activation and blood–brain barrier integrity after ischemia, so we investigated whether inhibiting the ACP, which we have shown improves acute survival after stroke (Alawieh et al., 2015b), reduced hemorrhagic transformation. Mortality rate at 24 h after ischemia was significantly higher in vehicle groups compared with CR2fH-treated groups (27.1% vs 10.1%, $p < 0.01$). Of 32 vehicle-treated animals that died within 24 h after MCAO, 56% of deaths were associated with intracerebral hemorrhage compared with 11% of deaths in CR2fH-treated animals (proportion comparison, $p < 0.01$; Fig. 1*a*). We confirmed that reduced hemorrhage is due to inhibition of the ACP by demonstrating that hemoglobin content in the ipsilateral hemisphere was significantly and similarly reduced by CR2fH treatment or factor B deficiency (fB is an ACP protein) (Fig. 1*b*,*c*). Levels of the complement activation products, C3a and C5a, were significantly elevated in controls at 12 h after stroke and were significantly reduced by CR2fH treatment or fB deficiency (Fig. 1*d*,*e*). There was a significant positive correlation between C3a and C5a levels and hemoglobin content in the brain (Fig. 1*f*). We also confirmed our previous finding that inhibition or deficiency of the ACP significantly reduced infarct volume acutely after MCAO (Fig. 1*g*). Because hemorrhagic transformation is most likely to occur within the first 24–48 h after MCAO and is an uncommon event (<20% of total animals), animals dying within 2 d of MCAO were excluded from studies. There was no significant difference in survival between CR2fH or vehicle beyond 2 d of reperfusion (Fig. 1*h*).

Inhibition of the ACP but not rehabilitation therapy reduces lesion size after stroke

To assess the individual and combined effect of ACP inhibition and rehabilitation on evolution of infarct after stroke, mice were treated with CR2fH 90 min after MCAO and, after 48 h, were randomized to regular or rehabilitation cages (enriched environment, see Materials and Methods). T2-weighted MRI, diffusion tensor imaging (DTI), and diffusion kurtosis imaging (DKI) were used to track lesion and ipsilesional changes at days 4 and 14 after MCAO. Treatment with CR2fH alone or in combination with rehabilitation significantly reduced lesion volume as measured by T2 hyperintensity at days 4 and 14 after injury (Fig. 2*a*,*b*). Vehicle controls showed large infarcts that involved the basal ganglia, hippocampus, and ipsilateral cortex, whereas animals treated with CR2fH had minimal expansion of injury from the basal ganglia, the site of initial injury. MRI findings were further validated by Nissl staining of serial sections of the brain. CR2fH or CR2fH combined with rehabilitation reduced tissue loss, cellular infiltrate, and gliosis compared with vehicle and rehabilitation alone (Fig. 2*c*,*d*). Mapping of Nissl images to Paxinos' brain atlas further revealed that inhibition of CR2fH, with or without rehabilitation therapy, significantly reduced hippocampal, cortical, and striatal damage and damage and gliosis of white matter descending fibers (Fig. 2*c*,*d*). The anatomical pattern of injury in vehicle controls supports the occurrence of secondary expansion given the involvement of posterior structures (hippocampus) innervated by the posterior cerebral artery rather than MCA in rodents (Xiong et al., 2017). We used MRI to further investigate secondary damage between poststroke days 4 and 14.

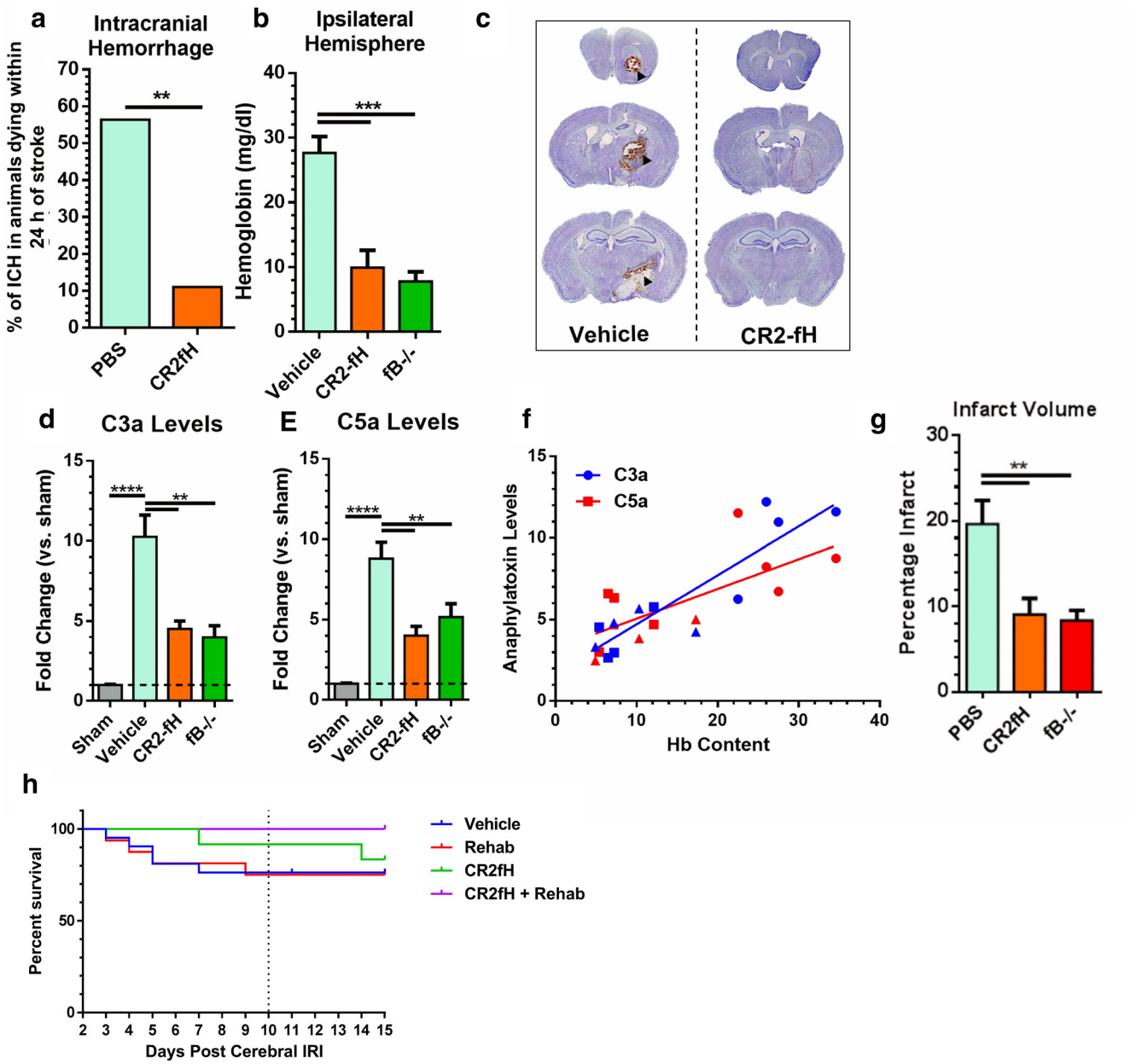

Figure 1. CR2fH treatment reduces intracranial hemorrhage and infarct acutely after stroke. ***a***, Percentage of animals dying within 24 h of stroke that had intracranial hemorrhage between vehicle- and CR2fH-treated animals. Population proportion statistic, $^{**}p < 0.01$. ***b***, CR2fH treatment and fB deficiency significantly reduce hemoglobin content in the ipsilateral hemisphere 12 h after MCAO compared with vehicle. One-way ANOVA, Dunnett's multiple comparisons. $n = 4$/group, $^{***}p < 0.001$. ***c***, Representative images of Nissl-stained brain sections showing peri-infarct intracerebral hemorrhage in vehicle controls but not in CR2fH-treated animals (90 min after MCAO administration). ***d***, ***e***, C3a and C5a ELISAs showing a significant reduction of MCAO-induced C3a and C5a generation by CR2fH treatment (90 min after MCAO administration) or fB deficiency 24 h after MCAO. One-way ANOVA, Tukey's multiple comparisons. $n = 4$/group, $^{****}p < 0.0001$, $^{**}p < 0.01$. ***f***, Correlation of hemoglobin content in the ipsilateral hemisphere with C3a levels (blue line, Pearson's correlation $r^2 = 0.800$, $p < 0.001$) and C5a levels (red line, Pearson's correlation $r^2 = 0.5071$, $p < 0.001$). ***g***, Both CR2fH treatment and fB deficiency significantly reduced acute infarct volume quantified from Triphenyl tetrazolium chloride-stained 2-mm-thick brain slices 24 h after stroke. ***h***, Mortality after MCAO and randomization to rehabilitation or regular housing. Kaplan–Meyer curve shows no significant difference between the groups. $n = 21$ vehicle, $n = 16$ rehabilitation, $n = 12$ CR2fH, and $n = 12$ CR2fH + rehabilitation.

DTI and DKI provide insight into microstructural changes in white and gray matter during inflammation and structural brain changes after ischemia (Hui et al., 2012; Umesh Rudrapatna et al., 2014). DTI and DKI series were acquired 4 and 14 d after injury to assess the evolution of degenerative changes in the lesion core and peri-infarct tissue. ROIs were selected from the ischemic core (basal ganglia area) and ipsilesional hippocampal and cortical areas and their symmetrical locations in the noninfarcted hemisphere by a person blinded to condition. At each time point, MD and MK are reported as ratios of ipsilateral to contralateral ROIs. In vehicle-treated animals, stroke resulted in decreased ipsilateral MD (ipsilateral/contralateral ratio <1; Fig. 2*e*,*f*) and increased ipsilateral MK (ipsilateral/contralateral ratio <1; Fig. 2*e*,*f*) in both the basal ganglia (injury core) and the hippocampus (perilesion) at day 4 after injury compared with contralateral ROI (Fig. 2*e*,*f*, $p < 0.05$ for ratios compared with 1 in vehicle group) which is similar to previous findings (Weber et al., 2015). In contrast to vehicle, CR2fH treatment alone or in combination with rehabilitation resulted in a normalization of MD and MK ratios at day 4 after MCAO (Fig. 2*f*). Rehabilitation alone nonsignificantly al-

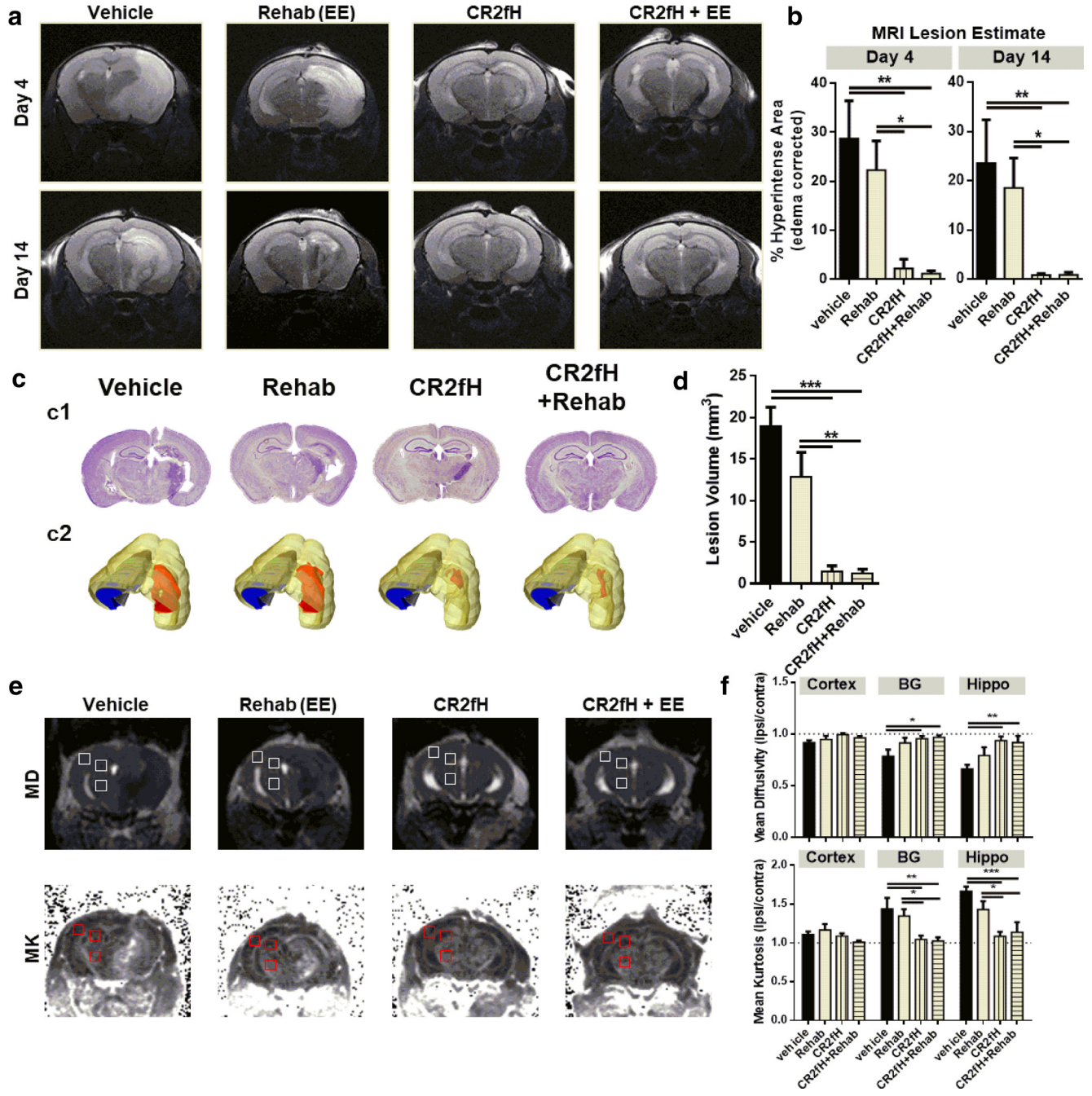

Figure 2. CR2fH treatment, but not rehabilitation (enriched environment and skilled handling), significantly reduced infarct size and scarring after MCAO. ***a***, Representative T2-weighted MRI images at days 4 and 14 after MCAO showing large hyperintense lesions in vehicle- and rehabilitation-treated animals compared with CR2fH-treated animals with or without rehabilitation therapy. ***b***, Quantification of ***a*** showing significant reduction of hyperintense lesion volume with CR2fH treatment compared with vehicle. Rehabilitation alone resulted in minimal reduction in lesion volume, which did not reach statistical significance. Kruskal–Wallis test with Dunn's multiple comparisons. $n = 6$ vehicle, $n = 8$ CR2fH, $^{*}p < 0.05$. $^{**}p < 0.01$. ***c***, Representative Nissl-stained brains showing secondary injury and scarring in the ipsilateral hemisphere 15 d after MCAO that was inhibited by acute CR2fH therapy. ***c1***, Nissl-stained brain slices. ***c2***, 3D rendering of lesion (in red) on a brain showing the location of cortex (yellow), basal ganglia (green), white matter (gray), and hippocampus (blue). ***d***, Quantification of lesion volume confirming histologically that CR2fH reduces secondary scarring 15 d after MCAO, with minimal contribution of rehabilitation therapy alone to reduced scarring. One-way ANVOA with Bonferroni's correction. $n = 8$/group, $^{**}p < 0.01$, $^{***}p < 0.001$. ***e***, Representative DTI and DKI images showing that CR2fH reduced MD and increased MK in the ipsilateral basal ganglia and hippocampus at day 4 after MCAO. ***f***, Quantification of ***e*** using three ROIs drawn over the cortex, hippocampus, and basal ganglia both ipsilaterally and contralaterally. Shown in ***e*** are contralateral ROIs. Rations of ipsilateral to contralateral MDs and MKs are compared. Two-way ANOVA, Bonferroni's correction, $n = 6$ vehicle, $n = 8$ CR2fH, $^{*}p < 0.05$, $^{**}p < 0.01$, $^{***}p < 0.001$.

tered MD and MK ratios compared with vehicle controls. There were no differences in MD or MK ratios in peri-infarct cortex in any group 4 d after MCAO. No differences were seen in MD or MK ratios at 14 d after injury across the four groups, similar to previous reports. These data indicate that inhibition of the ACP promotes normalization of DTI and DKI metrics in the injury core and ipsilesional area compared with vehicle treatment, suggesting a reduction in microstructural dysfunction. Stroke-related decreases in MD and increases in MK have been associated with increases in gliosis, inflammation, and demyelination (Zhuo et al., 2012; Falangola et al., 2014; Weber et al., 2015). Therefore, these data suggest CR2fH results in a faster resolution

of inflammatory changes in the brain during the first 4 d after MCAO. The rehabilitation paradigm used in this study did not, alone, significantly influence this process.

Synergistic improvement of motor and cognitive outcomes with combination therapy

We used a battery of motor and cognitive tasks to assess long-term function after MCAO in animals treated with CR2fH and/or rehabilitation therapy (Fig. 3*a*). Animals receiving rehabilitation alone had no significant reduction in neurological deficit, a measure of overall functional recovery, compared with vehicle controls (Fig. 3*b*). However, animals treated with CR2fH had significant reductions in deficit starting 2 d after MCAO and persisting throughout 15 d of recovery. Significant reductions in neurological deficit were seen whether animals were treated with CR2fH at 90 min, 6 h, or 24 h after MCAO (Fig. 3*b–e*). When combined with rehabilitation, CR2fH treatment resulted in a significantly earlier recovery from deficits and a more robust reduction in deficits on all tasks compared with CR2fH treatment alone. Comparing deficit scores between days 2 and 15 after MCAO, combination therapy, but not CR2fH or rehabilitation alone, resulted in a significant amelioration of deficits between the two time points (Fig. 3*f*). These data indicate that the major neuroprotective effects of CR2fH are elicited acutely, whereas rehabilitation provides an additional effect during recovery only when combined with CR2fH. The exception was animals treated with CR2fH 24 h after MCAO; these animals displayed a significant improvement between days 2 and 15 in the absence of rehabilitation, likely due to the acute effects of CR2fH treatment (Fig. 3*f*). One potential explanation for why combination therapy results in a significantly better recovery is that CR2fH improves early motor capacity, allowing animals to better engage with a rehabilitation environment. Indeed, animals treated with CR2fH spent significantly more time interacting with toys and running and explored more toys per session at day 3 after MCAO compared with vehicle controls (Fig. 3*g*). To further characterize motor recovery using more sensitive tasks, we used corner task as a measure of forelimb asymmetry, open-field activity to assess ambulation, and pasta handling as a measure of skilled forearm movement (Fig. 3*h–m*). As expected, performance at early time points (2–3 d after MCAO) was significantly improved in CR2fH-treated animals, with or without rehabilitation compared with vehicle controls. However, in contrast to the lack of rehabilitation alone effects on lesion size (Fig. 2), rehabilitation resulted in a significant improvement in motor performance starting on day 5 in the open-field task and on day 7 in the corner and pasta-handling tasks. CR2fH alone resulted in significant improvements throughout the 15 d of testing compared with vehicle controls and, despite having an overall more significant effect compared with rehabilitation only, there was no statistically significant improvement in CR2fH-treated animals compared with rehabilitation alone groups in the corner and pasta-handling tasks (Fig. 3*h–m*). However, combination of CR2fH and rehabilitation significantly improved performance on all tasks compared with both vehicle and rehabilitation alone (Fig. 3*h–m*).

We also assessed recovery of cognitive capacity in which secondary injury contributes to hippocampal damage. We used the Barnes maze to assess spatial learning and retention of learned memory during the second week after MCAO. Compared with individual treatments and vehicle control, animals receiving combined therapy had significantly faster learning curves and better retention, as measured by the total path before reaching the escape hole and the number of error pokes (Fig. 4*a–c*). Rehabilitation alone- and CR2fH alone-treated mice showed a significant improvement compared with vehicle and CR2fH alone provided a significant improvement compared with rehabilitation alone. A similar outcome pattern was also observed on the passive avoidance task, which assesses the ability of animals to retain avoidance memory learned before MCAO (Fig. 4*d*). A summary of motor and cognitive outcome measures is provided in Table 1. To provide a quantitative assessment of the overall recovery process, acute, subacute, and long-term performance on motor and cognitive tasks for individual animals were used to perform a PCA of variance (Fig. 4*e*). We identified three PCs that explained 99.2% of the variance and showed that combined therapy with CR2fH and rehabilitation resulted in the greatest reduction in impairments, bringing animals close to sham levels of performance (Fig. 4*e*). We also performed PCA analysis on motor and cognitive tasks separately and demonstrated that the impact of rehabilitation therapy was more pronounced on cognitive performance (Fig. 4*f*, right) compared with motor recovery (Fig. 4*f*, left), whereas CR2fH had comparable effects on both aspects of recovery (Fig. 4*f*).

To follow preclinical recommendations to investigate experimental neuroprotective approaches in aged mice, we investigated the interplay between rehabilitation and complement inhibition in 14-month-old mice (Fig. 5*a*,*b*). Animals were followed only through 10 d of recovery because vehicle-treated aged animals did not survive beyond day 10, although CR2fH treatment significantly improved the 10 d survival of aged animals (Fig. 5*b*). Similar to adult mice, CR2fH and combination therapy, but not rehabilitation alone, significantly improved functional recovery in aged animals (Fig. 5*a*,*b*). Although there was a trend indicating that combined therapy improved outcome compared with CR2fH alone, the difference did not reach statistical significance. This may be due to the lower capacity of aged mice to engage in rehabilitation strategies, as well as lower neuronal capacity for regeneration and reorganization in aged mice (Tennant et al., 2015). We additionally demonstrated that CR2fH is protective in female mice, with significant improvements in long-term deficits and a reduction in long-term mortality (Fig. 5*c*,*d*).

Chronic neuroinflammation after stroke is mildly reduced by rehabilitation but robustly inhibited by CR2fH

We next investigated the effect of rehabilitation on complement activation and whether the effect of CR2fH treatment on improving rehabilitation-dependent outcomes is, at least in part, due to a rapid resolution of inflammation that allows for more effective rehabilitation-induced regenerative mechanisms. We demonstrated persistent deposition of both IgM and C3d in the infarcted hemisphere surrounding the astrogliotic lesion, as well as along the endothelium of perilesional vessels, 15 d after MCAO (Fig. 6*a–d*). In CR2fH-treated animals, there was a significant reduction and near absence of IgM and C3d deposition in the ipsilateral hemisphere with or without rehabilitation. Interestingly, rehabilitation alone resulted in a mild but significant decrease in IgM and C3d deposition (Fig. 6*c*,*d*). We also assessed the extent of astrogliotic scarring using GFAP staining for astrocytosis and Mac2 (Galectin-3) staining for proliferating microglia/macrophages. The extent of astrogliotic scarring in the different groups reflected the extent of IgM and C3d deposition (Fig. 6*e–g*). CR2fH significantly reduced astrocytic and microglia/macrophage activation in the infracted hemisphere, whereas rehabilitation alone had a more modest effect on astrogliotic scarring 15 d after injury (Fig. 6*e–g*). To support and extend these findings, we performed high-throughput gene expression analysis using a

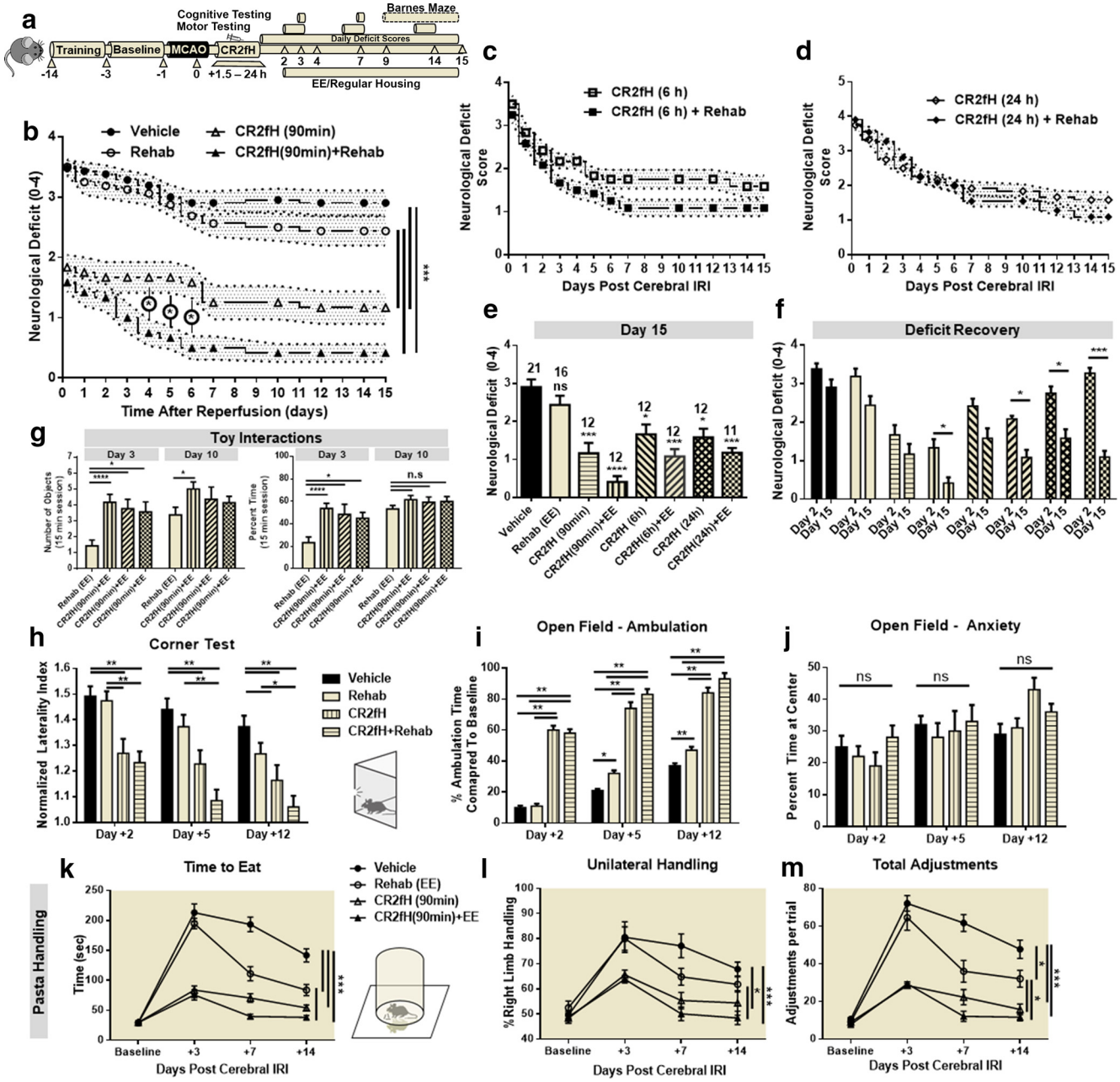

Figure 3. Combination of CR2fH treatment and rehabilitation therapy resulted in faster and more pronounced motor recovery 15 d after MCAO. ***a***, Overview of the experimental design. Survival curve for different groups is shown in Figure 1*h*. ***b***, CR2fH administered 90 min after ischemia with or without rehabilitation resulted in significant and sustained improvement in neurological deficit over 15 d of recovery compared with vehicle or rehabilitation therapy alone. Compared with CR2fH alone, the CR2fH + rehabilitation group exhibited significantly faster recovery during the first week after MCAO. Two-way ANOVA, Bonferroni's correction, $n = 11–21$/group (individual n's are shown in Fig. 2*e*). $^{*}p < 0.05$, $^{***}p < 0.001$. ***c***, ***d***, CR2fH also improved recovery of functional deficits when administered 6 h (***c***) or 24 h (***d***) after MCAO. ***e***, Comparison of neurological deficits at day 15 after injury showing that CR2fH significantly improved long-term functional recovery compared with vehicle and that, when combined with rehabilitation, more pronounced recovery is observed. Comparisons were made against vehicle group. Kruskal–Wallis test with Dunn's multiple comparisons, not significant (ns), $^{*}p < 0.05$, $^{***}p < 0.001$, $^{****}p < 0.0001$. ***f***, Pairwise comparison of functional recovery between days 2 and 15 across the different groups showing that, despite significant acute improvement achieved with CR2fH alone compared with vehicle, combination of CR2fH with rehabilitation, but not CR2fH or rehabilitation alone, resulted in more pronounced recovery beyond the acute phase (between days 2 and 15). Two-way ANOVA with Bonferroni's correction, $n = 11–21$/group, $^{*}p < 0.05$, $^{***}p < 0.001$. ***g***, Among animals treated with rehabilitation, animals cotreated with CR2fH showed significantly more interaction with the enriched environment compared with vehicle-treated animals at day 3, but not day 10, after MCAO. Two-way ANOVA with Bonferroni's correction, $n = 16$ vehicle, $n = 12$ CR2fH 90 min, $n = 7$ CR2fH 6 and 24 h, $^{*}p < 0.05$.$^{***}p < 0.001$. ***h***, ***i***, During the first week of recovery, CR2fH (90 min) alone or with rehabilitation significantly reduced forelimb asymmetry on the corner test (***h***) and increased open-field locomotor activity (***i***) compared with vehicle. Combination treatment has the largest effect on both tasks at any time point. ***j***. No difference among groups was seen in the percentage time spent at center, thus controlling for potential difference in anxiety levels between the groups. Two-way ANOVA with Bonferroni's correction, $n = 21$ vehicle, $n = 16$ rehabilitation, $n = 12$ CR2fH ± rehabilitation, $^{*}p < 0.05$, $^{**}p < 0.01$, $^{***}p < 0.001$. ***k***–***m***, On pasta-handling task, animals treated with rehabilitation, CR2fH, or CR2fH + rehabilitation showed signs of improvement in time to eat compared with vehicle (***k***), but the improvement in unilateral handling and number of adjustments was only significant in CR2fH ± rehabilitation animals compared with vehicle controls. Two-way ANOVA with Bonferroni's correction, $n = 8$/group, $^{*}p < 0.05$, $^{**}p < 0.01$, $^{***}p < 0.001$.

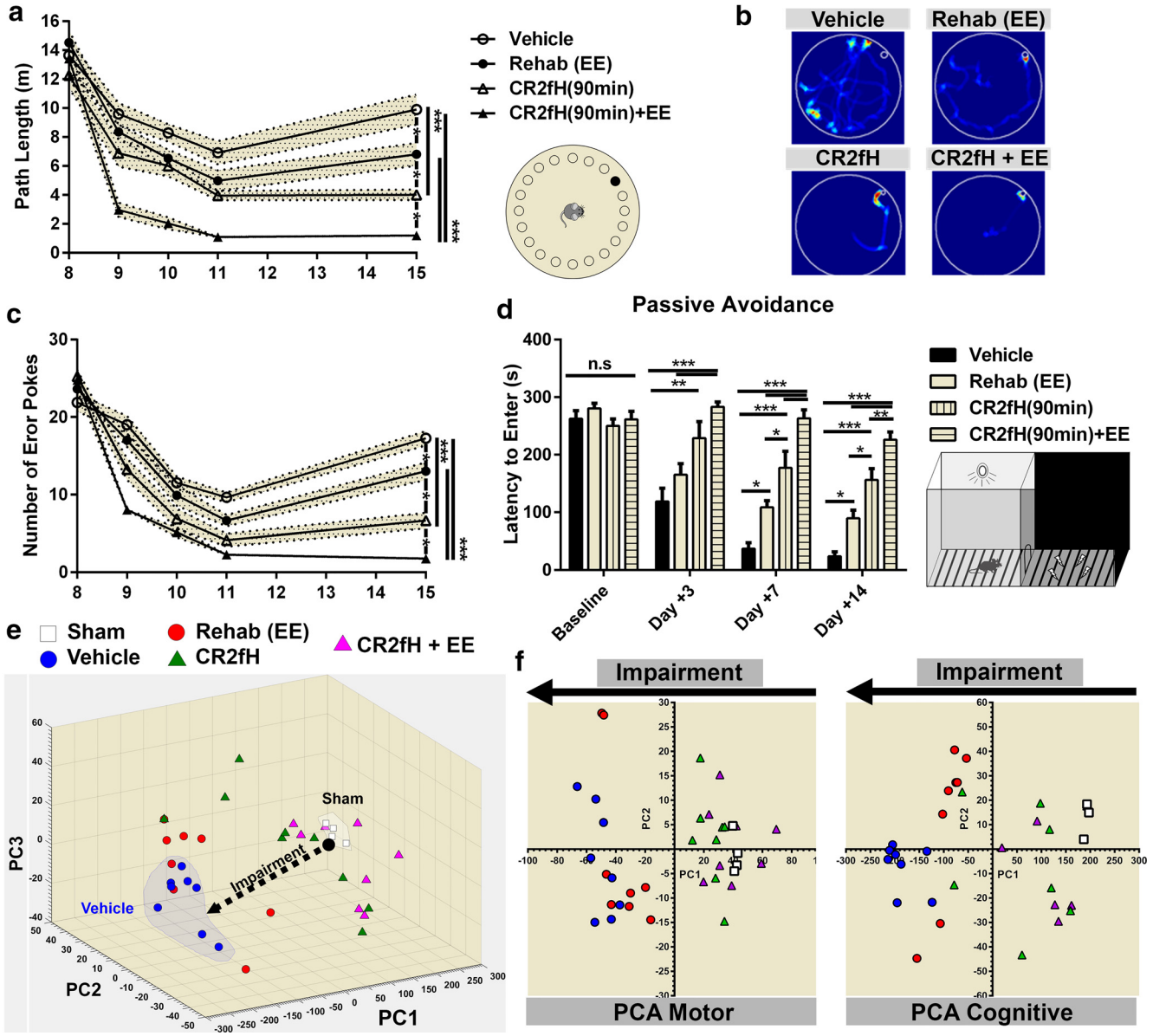

Figure 4. Improvement in cognitive performance after MCAO with rehabilitation, CR2fH, and combination therapy. ***a–c***, CR2fH treatment alone or in combination with rehabilitation significantly improved spatial learning (days 9–11 after MCAO) and retention of learned memory (day 15 after MCAO) compared with vehicle controls, as assessed by the total path length before reaching the target hole (***a***) or the number of error pokes (***c***). Cotreatment with CR2fH and rehabilitation also reduced path length and number of errors significantly compared with rehabilitation alone during learning. At the retention phase, rehabilitation alone showed significant improvement in both measures compared with vehicle, whereas CR2fH + rehabilitation was significantly better than CR2fH alone. Statistical results of retention day are displayed. Two-way ANOVA, Bonferroni's correction, $n = 8$/group, $^{*}p < 0.05$, $^{***}p < 0.001$. Results of multiple comparisons: (1) day 8: no significant difference between groups; (2) day 9: vehicle versus CR2fH: $p < 0.05$, vehicle versus CR2fH + rehabilitation: $p < 0.001$, rehabilitation or CR2fH versus CR2fH + rehabilitation: $p < 0.01$; (3) day 10: vehicle versus CR2fH: $p < 0.001$, all groups compared with CR2fH + rehabilitation: $p < 0.001$; (4) day 11: vehicle versus CR2fH: $p < 0.05$, all groups compared with CR2fH + rehabilitation: $p < 0.001$; and (5) day 15: displayed on graph. ***d***, Passive avoidance task revealed that animals treated with CR2fH with or without rehabilitation have better memory retention (longer time to enter the shock chamber) compared with vehicle and rehabilitation alone starting 7 d after MCAO. At both 7 and 14 d after injury, CR2fH was significantly better than rehabilitation alone. Rehabilitation alone was significantly better than vehicle, but combination therapy was significantly superior to all other groups. Two-way ANOVA, Bonferroni's correction, $n = 8$/group, $^{*}p < 0.05$, $^{**}p < 0.01$, $^{***}p < 0.001$. ***e***, PCA of the performance on the different motor and cognitive tasks displayed in Figures 2 and 3 (see Materials and Methods) showed that three PCs (PC1–PC3) can explain 99.2% of the variance. Individual animal data including shams were plotted against the three PCs, showing that CR2fH combined with rehabilitation was most efficient at bringing the animals closer to sham compared with either single therapy. ***f***, PCA analysis performed only on motor (right) or cognitive tasks (left) indicate that the effect of rehabilitation was more pronounced on cognitive rather than motor tasks. Two PCs explaining ~90% of the variance were plotted.

Nanostring immunology gene panel to investigate genes dysregulated by MCAO and their alteration by our therapeutic interventions (Fig. 7). Using hierarchical clustering and PCA analysis of differentially expressed genes, we demonstrated that, after MCAO, vehicle-treated animals had a unique signature of upregulated immunology-related genes (Fig. 7*a*,*b*). As assessed by GO enrichment analysis, genes upregulated by MCAO belong to the biological processes of the following: (1) IFN-γ signaling required for cell-mediated response and microglia/macrophage activation, (2) cell adhesion and migration, and (3) complement activation (Fig. 7*c*). Rehabilitation, CR2fH treatment and combined therapy normalized the majority of gene signatures to a sham-like profile (Fig. 7*a–c*). Rehabilitation alone significantly reduced the expression of genes involved in complement activa-

Table 1. Summary of outcome measures

	Subacute outcome (5–7 d)				
Group	Functional deficit	Corner laterality	Locomotor activity	Pasta handling	Passive avoidance
Vehicle	− − − −	− − − −	+	+	+
Rehab	− − −	− − −	+ +	+ +	+ +
CR2fH	− −	− −	+ + + +	+ +	+ + +
Combined	−	−	+ + + +	+ + + +	+ + + +

	Chronic outcome (12–15 d)					
Group	Functional deficit	Corner laterality	Locomotor activity	Pasta handling	Passive avoidance	Barnes maze
Vehicle	− − − −	− − − −	+	+	+	+
Rehab	− −	− −	+ +	+ +	+ +	+ +
CR2fH	− −	−	+ + + +	+ +	+ + +	+ + +
Combined	−	−	+ + + +	+ + + +	+ + + +	+ + + +

−, Gradient of deficit; +, gradient of positive performance.

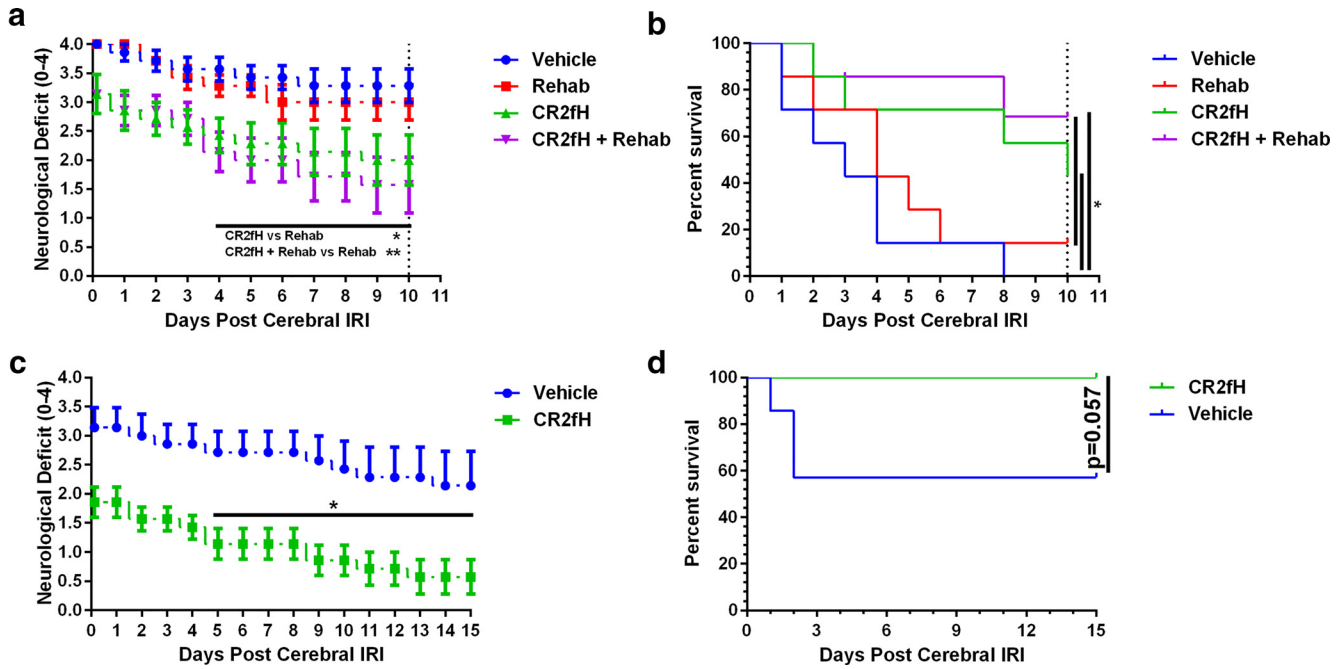

Figure 5. CR2fH (administered 90 min after MCAO) is also protective in female mice and aged male mice (14 months old). ***a***, CR2fH alone or in combination with rehabilitation significantly reduced neurological deficits in aged mice compared with vehicle; however, only CR2fH + rehabilitation was significantly better compared with rehabilitation only ($p < 0.05$). Two-way ANOVA, Bonferroni's correction, $n = 7$/group, $^*p < 0.05$, $^{**}p < 0.01$. ***b***, Survival was significantly improved by CR2fH with or without rehabilitation in aged animals after MCAO. Experiments were terminated at day 10 due to loss of all vehicle controls. Log–rank (Mantel–Cox) test, $n = 7$/group, $^*p < 0.05$. ***c***, ***d***, CR2fH improved neurological deficits and survival of adult female mice through 15 d after MCAO. ***c***, Two-way ANOVA, Bonferroni's correction, $n = 7$/group, $^*p < 0.05$, $^{**}p < 0.01$. ***d***, Log–rank (Mantel–Cox) test, $n = 7$/group. $p = 0.057$.

tion (C3), apoptosis (caspases 1 and 3), microglial and monocyte activation (Cxcl12, Ccl2), inflammatory cell activation (Cd24, Cd36, Tcf7), and cellular adhesion (Icam1) and significantly upregulated the expression of Ctla4 that is involved in negative regulation of immune cell activation (Fig. 7*e*). PCA analysis showed that gene expression in the infarcted hemisphere of CR2fH- and CR2fH + rehabilitation-treated mice had a closer proximity to sham patterns compared with rehabilitation alone, although rehabilitation alone reversed the upregulation of several MCAO-induced genes (Fig. 7*d*). In fact, reviewing individual gene panels revealed a significant effect of CR2fH and CR2fH + rehabilitation on reducing the expression of markers of microglia/macrophage activation (Fig. 7*f*), complement protein C3, and proteins of the ACP (Fig. 7*g*), indicating that inhibition of ACP by CR2fH interrupts a positive feedback loop of complement-mediated inflammation. Network analysis of pathways involved in attraction, activation, and proliferation of microglia and macrophages in the brain revealed that the combination of rehab and CR2fH resulted in downregulated expression of the majority of genes involved in these pathways, an effect that was more prominent than with rehabilitation alone (see Fig. 7-1, available at https://doi.org/10.1523/JNEUROSCI.0111-18.2018.f7-1, Fig. 7-2, available at https://doi.org/10.1523/JNEUROSCI.0111-18.2018.f7-2, and Fig. 7-3, available at https://doi.org/10.1523/JNEUROSCI.0111-18.2018.f7-3). This finding, along with the significant feedforward interaction mechanism between complement components and cytokines involved in activation of microglia/macrophages, reveals that treatment with CR2fH alone or CR2fH combined with rehabilitation resulted in the interruption of neuroinflammation (see Fig. 7-1, available at https://doi.org/10.1523/JNEUROSCI.0111-18.2018.f7-1, Fig. 7-2, available at https://doi.org/10.1523/JNEUROSCI.0111-18.2018.f7-2, and Fig. 7-3, available at https://doi.org/10.1523/JNEUROSCI.0111-18.2018.f7-3), which would otherwise have persisted for weeks after injury, as evidenced by the dense cellular infiltrate in the brain at 15 d after stroke (Fig. 6*e*,*f*).

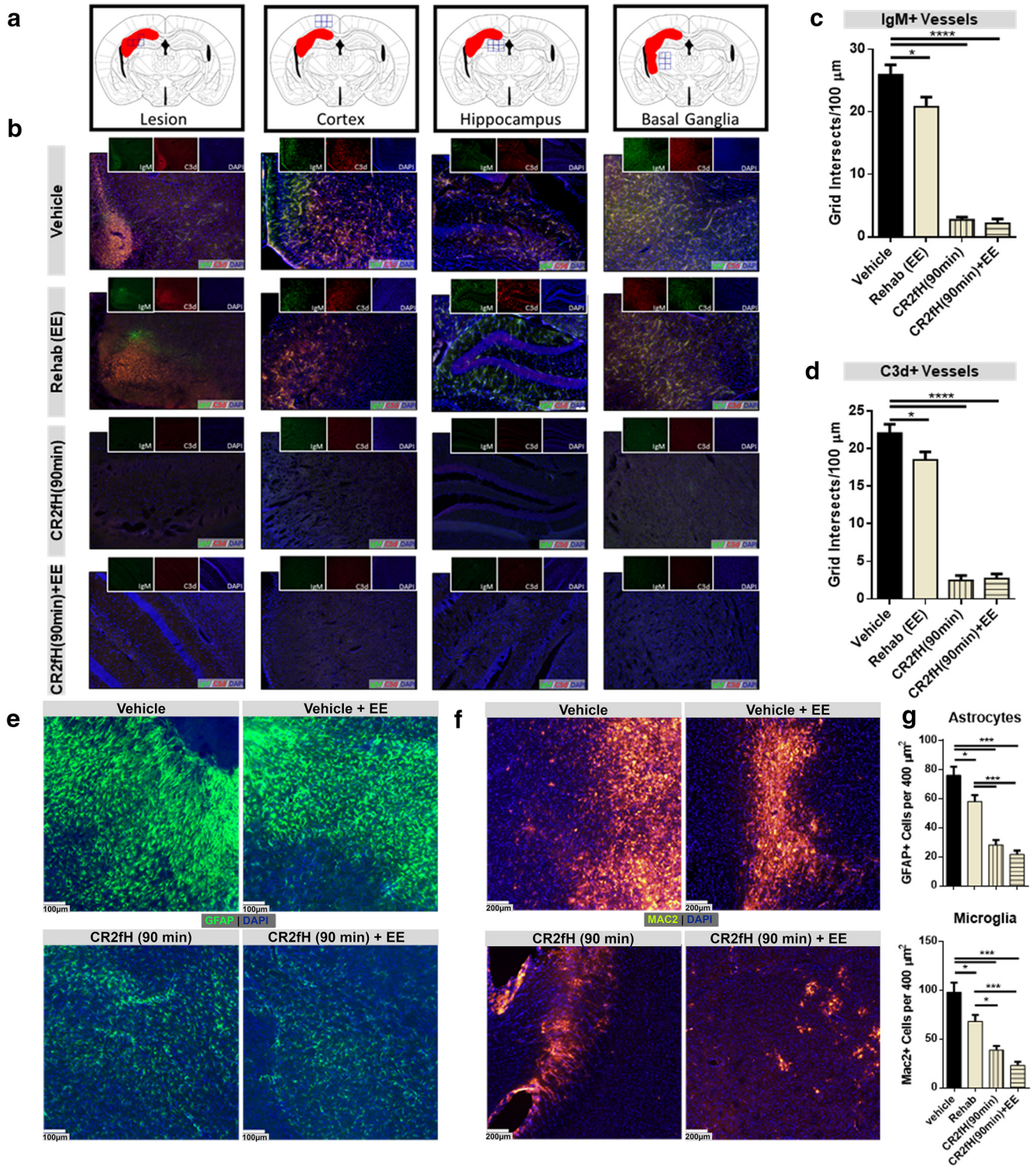

Figure 6. CR2fH treatment blocks a robust inflammatory response that otherwise propagates to the chronic phase after MCAO. ***a, b,*** A sustained neuroinflammatory response manifested by C3d and IgM deposition 15 d after MCAO was inhibited by a single acute administration of CR2fH (90 min after MCAO). Shown in ***a*** are the lesion locations and in ***b*** the different treatment groups. Green, IgM; red, C3d; blue, DAPI. ***c***, ***d***, Quantification of IgM (***c***) and C3d (***d***) deposition showing that CR2fH significantly reduced deposition of both markers on the inflamed ipsilateral endothelium. Rehabilitation alone resulted in a modest but significant reduction in IgM and C3d deposition by 15 d after MCAO. ANOVA with Bonferroni's correction, $n = 5$ animals (4 fields per animal chosen from the peri-infarct lesion), $^{*}p < 0.05$, $^{****}p < 0.0001$. ***e***, GFAP immunofluorescence staining showing extensive astrogliosis in the peri-infarct area 15 d after MCAO that was significantly inhibited by CR2fH therapy alone, but not by rehabilitation alone. ***f***, Mac2 immunofluorescence staining showing extensive gliosis and proliferation of M1-polarized (inflammatory type microglia/macrophages) in the perilesional area of vehicle- and rehabilitation-treated animals that was significantly inhibited by CR2fH therapy. ***g***, Quantification of ***e*** and ***f*** showing that, although CR2fH more robustly reduced astrocytosis and microgliosis, rehabilitation nevertheless had a milder though significant effect on reducing inflammatory phenotype 15 d after stroke. ANOVA with Bonferroni's correction, $n = 5$ animals (3 fields per animal), $^{*}p < 0.05$, $^{***}p < 0.001$.

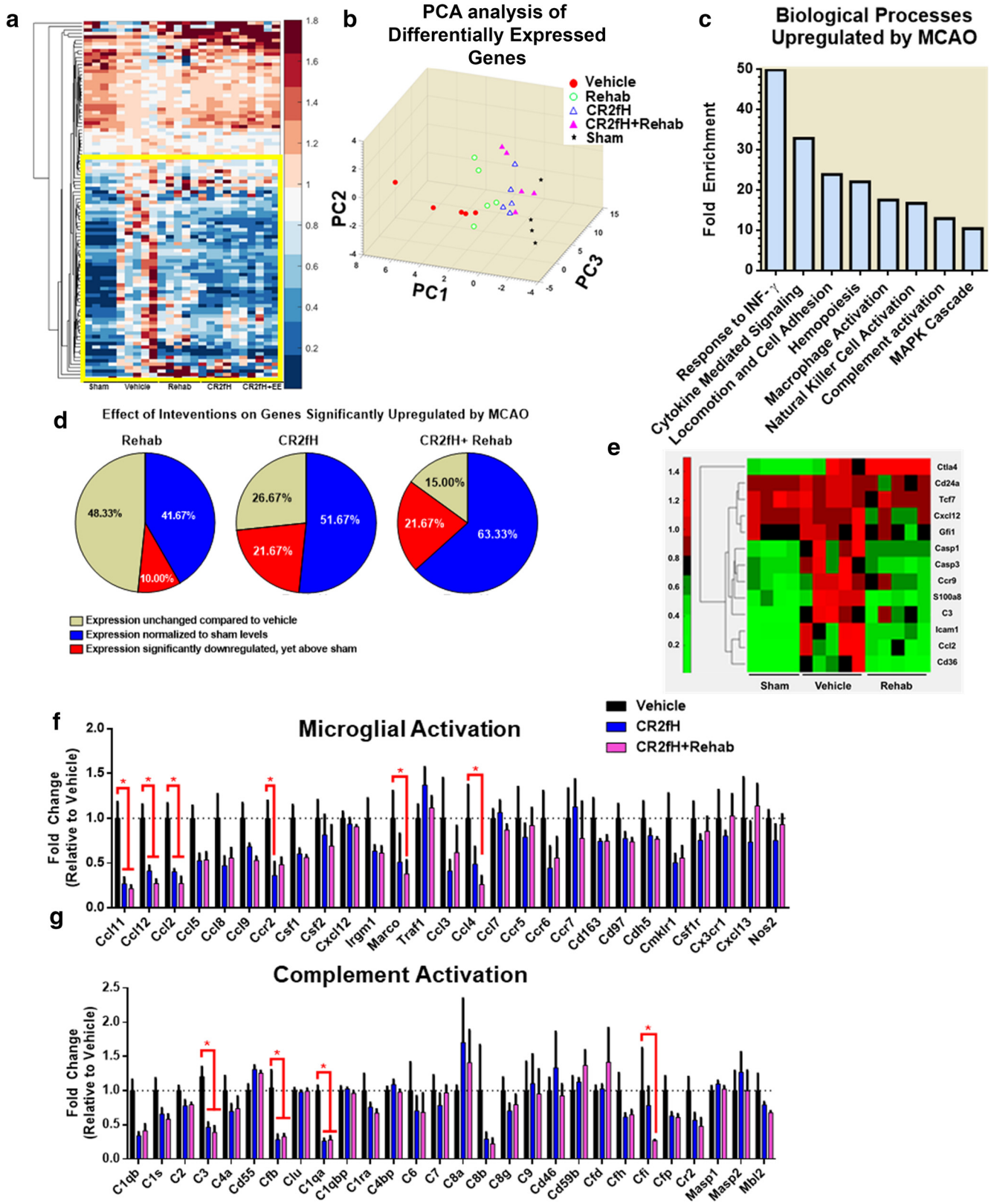

Figure 7. Gene expression analysis of the impact of CR2fH and rehabilitation on immune-related genes in the ipsilateral hemisphere 5 d after stroke. ***a***, Clustergram of differentially expressed genes on Nanostring immunology gene expression assay with a $p < 0.05$ on at least one comparison. A detailed network of gene expression changes is provided in Figure 7-1 (available at https://doi.org/10.1523/JNEUROSCI.0111-18.2018.f7-1), Figure 7-2 (available at https://doi.org/10.1523/JNEUROSCI.0111-18.2018.f7-2), and Figure 7-3 (available at https://doi.org/10.1523/JNEUROSCI.0111-18.2018.f7-3). ***b***, PCA of differentially expressed genes showing PC1–PC3, which explain 69% of the variance. ***c***, Enrichment analysis of GO biological processes enriched in genes that are significantly upregulated in MCAO versus sham animals. Enrichment statistics were performed through PANTHER (Mi et al., 2016). Processes with $p < 0.0001$ are displayed. ***d***, Clustergram of genes significantly upregulated or significantly downregulated in rehabilitation compared with vehicle ($p < 0.05$). ***e***, Pie charts showing the distribution of genes dysregulated by MCAO according to their changes by the different treatment categories. ***f, g,*** Gene expression panels of genes involved in microglial/macrophage activation (***f***) and complement activation (***g***). Two-way ANOVA, Bonferroni's correction, $n = 5$/group, $^*p < 0.05$.

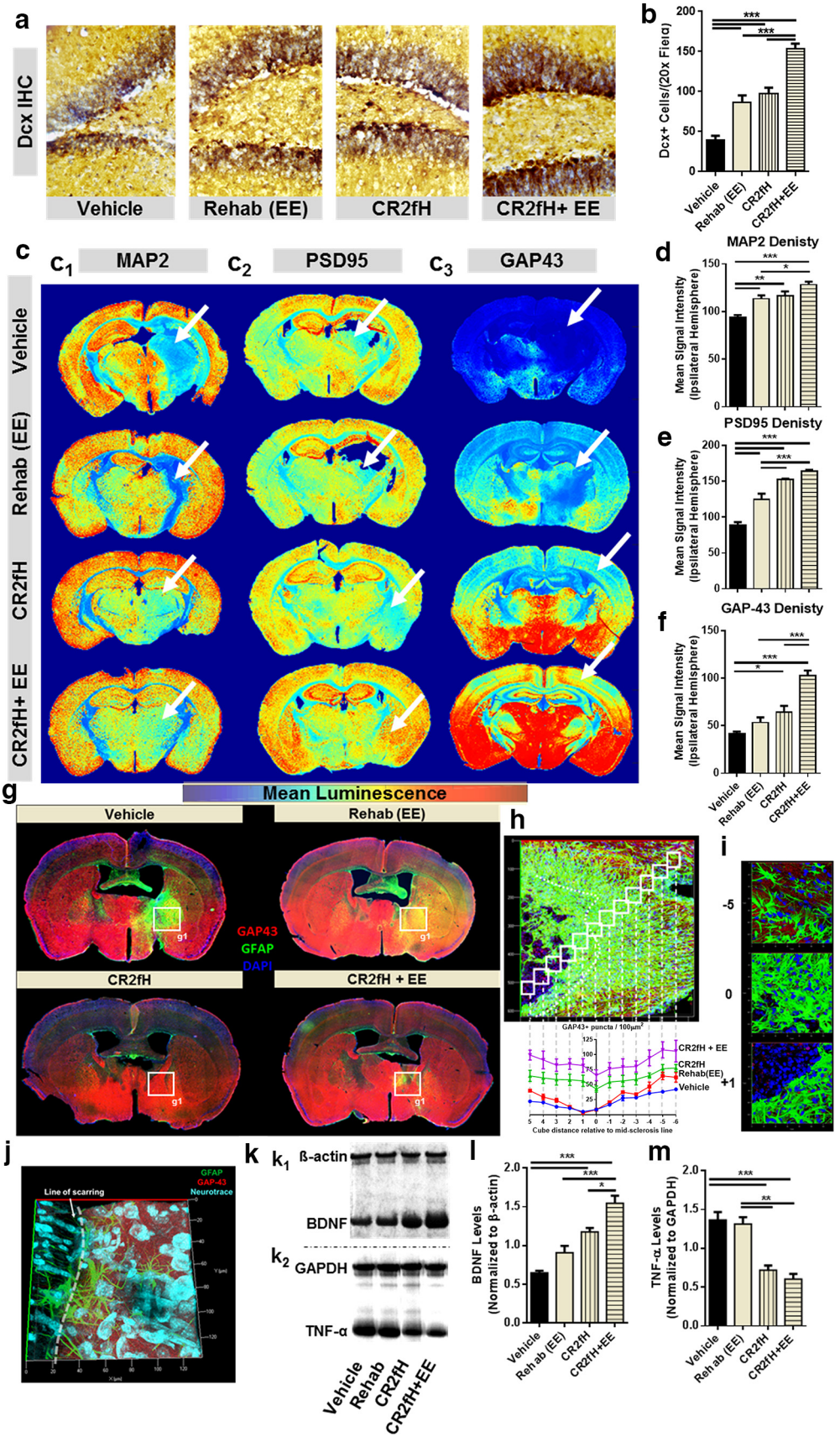

Figure 8. CR2fH removes the inhibition on regenerative mechanisms promoting the outcome of rehabilitation therapy. ***a***, Dcx immunostaining of perilesional hippocampi quantified in ***b*** showing a significant increase in the number of neuroblasts migrating to the ipsilateral hippocampus 15 d after injury with rehabilitation, CR2fH treatment, or combination therapy. However, combination of CR2fH and rehabilitation showed a more robust increase in Dcx+ cells compared with either single intervention. ANOVA. $n = 6$ animals (2 fields each), $^{***}p < 0.001$. ***c–f***, Immunostaining for markers of regeneration and remodeling, including dendritic arborization (MAP2), synaptic density (PSD-95), and axonal growth (GAP-43) of full-brain slices showing (*Figure legend continues.*)

CR2fH removes the inhibition on neuroregenerative processes after stroke

We next investigated the hypothesis that targeted inhibition of the ACP creates a permissive environment for spontaneous and rehabilitation-induced regenerative processes. Dcx is a marker of migrating neuroblasts and we assessed the incorporation of Dcx+ neurons into the ipsilaterally infarcted hippocampus 15 d after MCAO. Both CR2fH treatment and rehabilitation alone resulted in a higher number of Dcx+ cells in the hippocampus (Fig. 8*a*,*b*). Conversely, combination therapy resulted in a significantly higher increase in Dcx+ cells compared with either therapy alone, indicating that CR2fH and rehabilitation influence different cellular mechanisms. We then assessed neural reorganization and plasticity by analyzing the expression of proteins related to axonal growth (GAP43), dendrites (MAP2), and synapses (PSD95) 15 d after MCAO. Stroke resulted in a significant decrease in dendritic and synaptic density in the perilesional hemisphere (Fig. 8*c1*,*c2*), with a near absence of axonal growth (Fig. 8*c1*,*c2*). Both rehabilitation and CR2fH individually resulted in increased synaptic, dendritic, and axonal densities in the ipsilateral hemisphere (Fig. 8*c–f*). However, combination therapy further increased dendritic, axonal, and synaptic densities (Fig. 8*c–f*) and returned densities to levels that are almost comparable to the contralateral hemisphere (Fig. 8*c*), although the contralateral hemisphere also underwent reactive degenerative and regenerative effects. Indeed, combination therapy and individual therapies also resulted in increased densities of remodeling and regeneration markers in the contralateral hemisphere (Fig. 8*c*), although this could be due to the animal participating in bilateral tasks and the contralateral cortex being more permissive to experience driven plasticity.

To further investigate whether the synergistic effect of combination therapy is related to CR2fH-mediated reversal of inflammation-induced inhibition of recovery together with rehabilitation-induced neural remodeling, we costained for axonal growth (GAP43, a marker of regeneration) and astrogliosis (GFAP) (Fig. 8*g–j*). We found that substantial astrogliotic scarring produced a barrier that seemed to block the growth of GAP43+ fibers into the ischemic perilesional area, whereas rehabilitation alone did not affect the extent of scarring but increased the density of GAP43+ growing axons. Conversely, CR2fH treatment significantly reduced astrogliotic scarring, allowing for increased infiltration of growing axons into the perilesional brain (Fig. 8*g*,*h*). Combination therapy both reduced the peri-infarct astrogliotic barrier and increased GAP43 density in the perilesional area (Fig. 8*g*,*h*). Indeed, by tracking the density of GAP43+ puncta using super-resolution immunofluorescent microscopy, we found a significant decrease in the number of growing axons approaching and traversing the astrogliotic scar in vehicle- and rehabilitation-treated animals. However, CR2fH therapy prevented this decrease in GAP43+ puncta and allowed for greater neurite outgrowth and uniform neuronal density across the perilesional brain (Fig. 8*h*,*i*). The difference in axonal density in the peri-scarring region existed despite a comparable neuronal density (Fig. 8*j*). Because TNF-α is a major marker of chronic inflammation in the CNS and BDNF is a major growth factor involved in rehabilitation-induced regeneration, we analyzed the levels of these two opposing factors to further investigate how rehabilitation and CR2fH treatment interact during recovery. Rehabilitation alone resulted in a mild increase in BDNF levels and no change in TNF-α levels, whereas CR2fH significantly reduced TNF-α levels and increased levels of BDNF (Fig. 8*k–m*). Combined CR2fH treatment and rehabilitation resulted in a similar reduction in TNF-α levels, but there was a more pronounced increase in the level of BDNF (Fig. 8*k–m*), thus supporting the above hypothesis regarding the interplay of a CR2fH effect on inflammation-induced inhibition of recovery and the effect of rehabilitation on potentiation of regenerative processes.

CR2fH acts cooperatively with tPA therapy to limit acute mortality and improve motor and cognitive outcomes after embolic stroke

To assess the effect of complement on outcomes after tPA, we used a microembolic model of ischemic stroke (Alawieh et al., 2016). Two hours after the administration of emboli, mice were treated with tPA, CR2fH, or a combination of the two reagents. CR2fH significantly reduced acute mortality compared with vehicle treatment, but tPA alone did not significantly affect survival compared with vehicle (Fig. 9*a*). Examination of the brains extracted at the time of death showed significant intracranial hemorrhage in tPA-treated animals (data not shown). Combination of CR2fH and tPA significantly reduced acute mortality and reversed tPA-associated mortality over 15 d of recovery (Fig. 9*a*). All three treatment groups showed a significant reduction of infarct volume compared with vehicle treatment 15 d after emboli administration; however, combination therapy resulted in 80% reduction in infarct volume (Fig. 9*b*). Motor recovery was assessed using daily neurological scoring and the corner task as a measure of forearm laterality. Both tPA and CR2fH single treatments resulted in comparable reductions in acute neurological deficits compared with vehicle controls, but animals treated with CR2fH showed additional improvement in motor recovery during the first 7 d after stroke compared with animals treated with tPA alone (Fig. 9*c*). Combination therapy with tPA and CR2fH resulted in a significant reduction in motor deficit compared with individual treatments (Fig. 9*c*). The corner task revealed that forearm laterality was significantly improved by all three treatment strategies up to 7 d after stroke; however, only CR2fH therapy and combination therapy resulted in a significant sustained improvement compared with vehicle at 14 d after stroke (Fig. 9*d*).

←

(*Figure legend continued.*) that a combination of CR2fH and rehabilitation resulted in the most pronounced and significant increase in dendritic and axonal growth to the perilesional area with subsequent increase in synaptic density. Significant increase in regenerative markers was also seen in CR2fH-treated animals (all three markers) and in rehabilitation-only animals (MAP2 and PSD95). ANOVA, full hemispheres quantified, $*p < 0.05$, $**p < 0.01$, $***p < 0.001$. Heat map shows mean luminescence. ***g***, Costaining for GAP-43 and GFAP showing that robust astrogliosis inhibits the regrowth of regenerating (GAP-43+) axons into the perilesional area. CR2fH significantly reduced astrogliotic scarring, resulting in increased GAP-43 infiltration to perilesional brain, whereas CR2fH in combination with rehabilitation further increased the levels of GAP-43 in the perilesional areas. Rehabilitation-only animals showed limited GAP43 increase that was still blocked by astrogliosis. ***h***, Quantification of GAP-43 density in the perilesional area showing that vehicle and rehabilitation animals showed a significant reduction in GAP43 density surrounding the areas of astrogliosis compared with CR2fH with or without rehabilitation. $p < 0.01$ comparing vehicle or rehabilitation with CR2fH with or without rehabilitation at locations −2 to 3. Two-way ANOVA, $n = 3$/group. ***i***, Representative 3D-rendered fields from ***h*** at different positions relative to the astrogliotic scar. ***j***, Notable reduction in GAP43 was observed near the areas of astrogliosis in vehicle-treated animals despite comparable neuronal density across the boundaries of the scar (NeuroTrace, cyan). ***k***, Representative Western blots showing levels of neuronal growth factor (BDNF) and TNF-α across the different groups. ***l***, Both CR2fH and rehabilitation alone resulted in a significant increase in the levels of BDNF in the ipsilateral hemisphere compared with vehicle. However, combination therapy resulted in a more robust and significant increase compared with either single intervention. ANOVA, $n = 6$/group, $*p < 0.05$, $***p < 0.001$. ***m***, Rehabilitation did not influence the levels of TNF-α. However, CR2fH with or without rehabilitation significantly reduced the levels of TNF-α compared with rehabilitation or vehicle groups. ANOVA, $n = 5$/group, $**p < 0.01$, $***p < 0.001$.

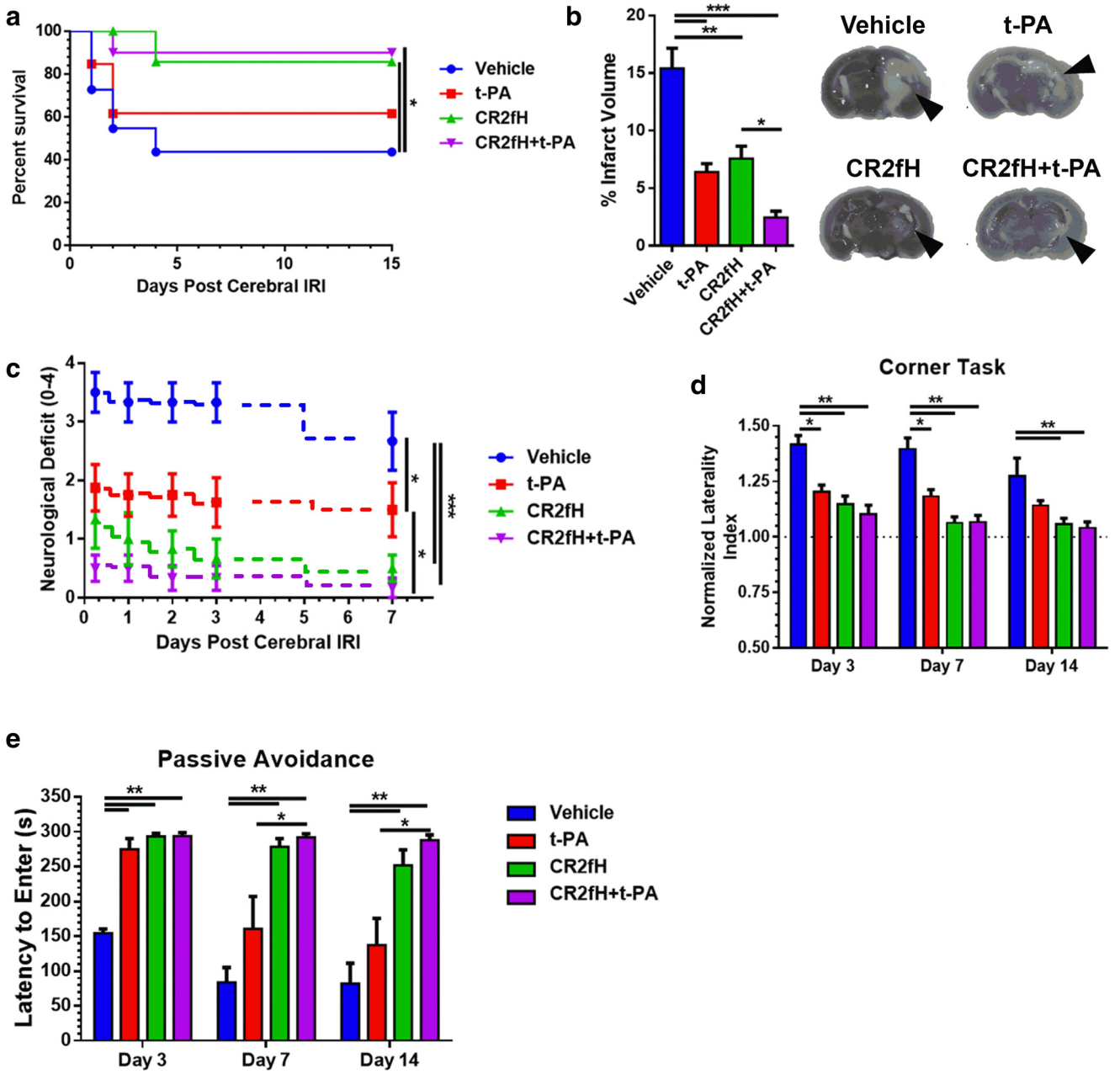

Figure 9. CR2fH acts cooperatively with tPA to reduce mortality and improve outcomes after embolic stroke. ***a***, Kaplan–Meyer curve of poststroke survival showing a significant reduction in mortality in animals treated with CR2fH or cotreated with CR2fH and tPA compared with vehicle treatment. Log–rank (Mantel–Cox) test, $n = 10–14$/group, $^{*}p < 0.05$. ***b***, Infarct volume was assessed using Nissl staining of serially cut brain sections 200 μm apart. tPA, CR2fH, and the combination significantly reduced infarct volume compared with vehicle. Combination of CR2fH and tPA resulted in the most profound effect in reducing infarct volume compared with single therapies. One-way ANOVA with Bonferroni's multiple comparisons. $n = 6$/group, $^{*}p < 0.05$, $^{**}p < 0.01$, $^{***}p < 0.001$. ***c***, Neurological deficit assessed daily starting 6 h after high-dose embolic stroke showed a significant additive effect of CR2fH and tPA therapy on overall deficit after stroke. Repeated-measures two-way ANOVA with Bonferroni's multiple comparisons, $n = 6–8$/group, $^{*}p < 0.05$, $^{***}p < 0.001$. Representative TTC-stained sections are also shown, with arrows indicating infarcted area. ***d***, Corner task was used to assess forearm laterality compared with baseline laterality before stroke. Similar to neurological deficits, combination therapy with CR2fH and tPA showed the most robust and sustainable effect in reducing deficits over 14 d of recovery compared with vehicle treatment. Two-way ANOVA with Bonferroni's multiple comparisons, $n = 6–8$/group, $^{*}p < 0.05$, $^{**}p < 0.01$. ***e***, Passive avoidance task was used to assess cognitive recovery after high-dose embolic stroke. On day 3 after emboli administration, animals treated with tPA, CR2fH, or a combination showed a significant improvement in memory retention (longer latency to enter the dark chamber) compared with vehicle controls. This improvement was only maintained at days 7 and 14 after stroke in animals treated with CR2fH and combination therapy, but not tPA alone. Two-way ANOVA with Bonferroni's multiple comparisons, $n = 6–8$/group, $^{*}p < 0.05$, $^{**}p < 0.01$.

In both human and experimental stroke, MCA occlusion is associated with cognitive deficits that include impairment in memory recall after stroke. We used the passive avoidance task to assess the ability of animals to retain and recall avoidance memory learned before stroke. Treatment with tPA, CR2fH, or a combination resulted in a significant increase in retention of avoidance memory at day 3 after stroke compared with controls (Fig. 9*e*). However, animals treated with tPA only were not able to sustain this retention beyond day 3 and did not show a significant increase in memory retention on days 7 and 14 after stroke (Fig. 9*e*). Conversely, CR2fH therapy and a combination of CR2fH and tPA resulted in sustained cognitive recovery and significantly

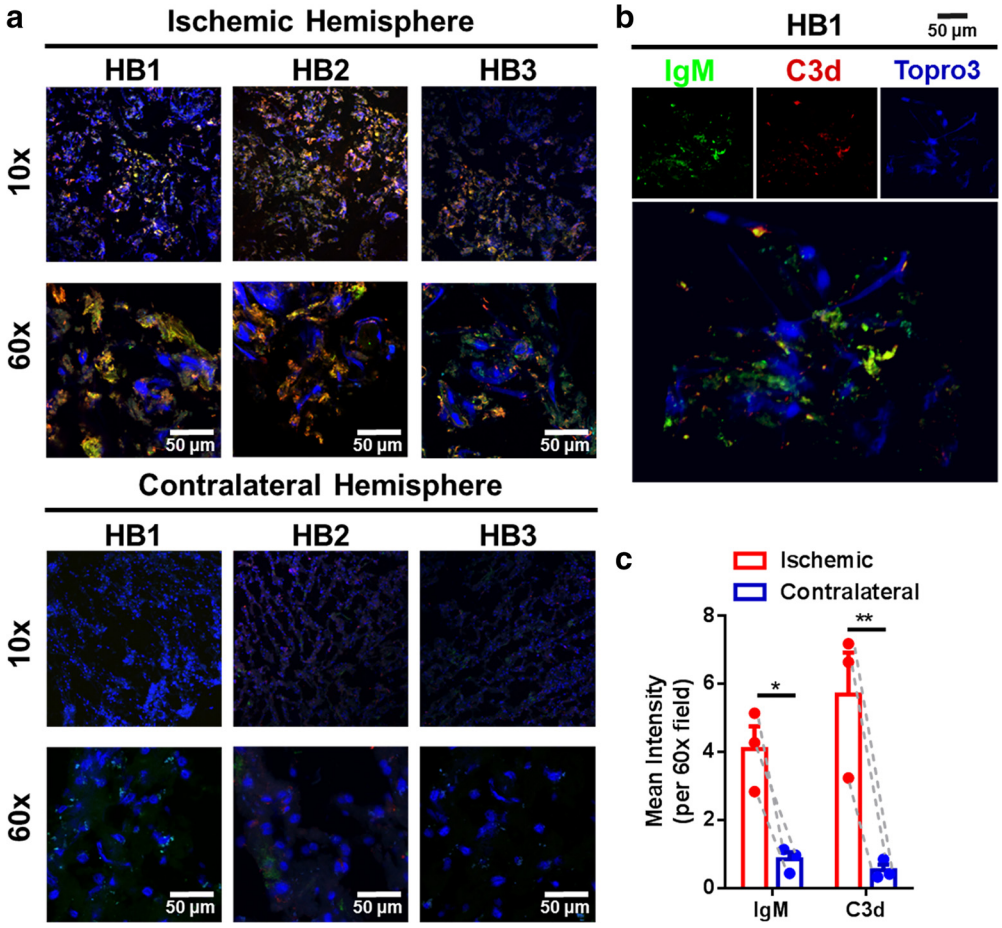

Figure 10. Complement and IgM deposition in the ischemic hemisphere of human patients who died from acute stroke. ***a***, Immunofluorescence microscopy showing IgM (green) and C3d (red) deposition in the ischemic but not contralateral hemisphere of patients who died from acute stroke. HB1, 24 h poststroke; HB2, 24–48 h poststroke; HB3, 48 h poststroke; blue, DAPI. ***b***, High-resolution 3D rendering of IgM and C3d deposition showing colocalization of C3d and IgM in the ischemic penumbra. ***c***, Pairwise comparisons of C3d and IgM deposition in the ipsilateral compared with the contralateral hemisphere showing significantly higher levels in the ipsilateral hemisphere of acute stroke patients. Pairwise two-way ANOVA, Bonferroni's correction, $n = 3$, $^{*}p < 0.05$, $^{**}p < 0.01$.

higher memory retention compared with controls 7 and 14 d after stroke.

CR2fH targeting epitope (C3d) is expressed in the ischemic human brain for several days after stroke

To address translational potential, we examined the temporal expression of C3d, the CR2fH-targeting ligand, in the human ischemic brain after stroke. Immunofluorescence microscopy demonstrated both C3d and IgM deposition in the perilesional area of postmortem brains from three patients who died from acute stroke. Furthermore, there was a similar pattern of C3d and IgM deposition in the perilesional area of human and murine brains (Fig. 10). The colocalization of IgM and C3d in human brains after stroke suggests a similar mechanism of IgM-mediated complement activation after ischemic stroke as has been demonstrated in mice (Elvington et al., 2012). There was continued and robust C3d expression in the perilesional area of human brains 72 h after stroke.

Discussion

We investigated the reciprocal interaction between complement activation and neurorehabilitation and tPA therapy during recovery after ischemic stroke. We show that rehabilitation reduces complement activation after stroke while enhancing regeneration and remodeling and that complement inhibition significantly enhances regenerative effects in a well established model of rehabilitation. The effect of rehabilitation on complement activation is a component of a mild, albeit significant, effect of rehabilitation on after stroke inflammation. However, a stronger and synergistic effect on long-term functional recovery after stroke was found with combined complement inhibition and rehabilitation. This effect can be explained by the fact that complement inhibition reduces neuronal loss, blocks chronic inflammation, and may render the microenvironment more sensitive to activity-dependent regeneration and remodeling. The coordinated interaction between rehabilitation and complement inhibition was bidirectional, such that rehabilitation therapy extended the post-stroke window of efficacy of CR2fH, resulting in near maximal recovery even when CR2fH was administered 24 h after MCAO. In parallel, CR2fH improved the response to rehabilitation therapy. Finally, we demonstrated that the safety and efficacy profile of tPA therapy, the only FDA-approved treatment for stroke, can be favorably altered with complement inhibition by reducing tPA-associated hemorrhage and potentiating the neuroprotective effects of tPA therapy.

Only a few studies have documented an anti-inflammatory effect of enriched rehabilitation (Ruscher et al., 2013; Yu et al., 2013). We show here that rehabilitation can modulate the expression of several proinflammatory genes, including complement

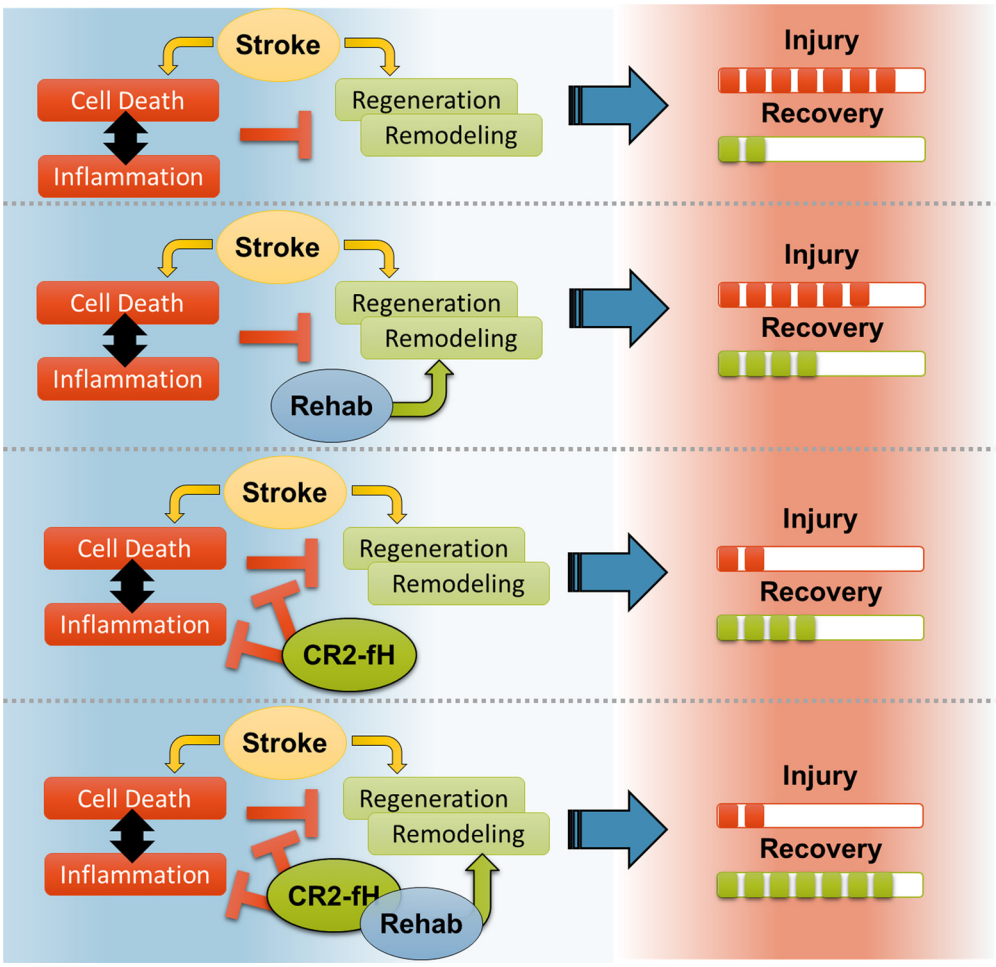

Figure 11. Illustration of the main hypothesis on how complement inhibition and rehabilitation interact to affect recovery after stroke.

genes, and can reduce complement deposition and inflammatory cell activation in the brain. Nevertheless, the anti-inflammatory effects of rehabilitation alone are mild compared with the effect of localized complement inhibition and are not sufficient to stop the evolution of neuroinflammation after stroke. We show that CR2fH inhibits the initiation and propagation of poststroke neuroinflammation, increases neuronal reserve available for engagement in the restoration of function, and lifts an inflammation-induced brake on regenerative responses. The cooperative interaction between complement modulation and rehabilitation, especially on regenerative processes, can be explained by the fact that CR2fH and rehabilitation influence the different cellular processes illustrated in Figure 11.

Although the role of complement in acute stroke has been well studied (Huang et al., 1999; Mocco et al., 2006), relatively few studies have investigated how complement modulates chronic outcomes and unexplored is how the complement system and rehabilitation therapy interact to shape poststroke recovery. Spontaneous and rehabilitation-induced functional recovery depends on many factors, including the extent and location of injury (Byblow et al., 2015) and the brain's ability to form new neurons or reorganize existing neural connections (Gauthier et al., 2012; Pekna et al., 2012). Limiting lesion size, upregulating neurogenesis, and enhancing poststroke neural plasticity can greatly reduce functional deficits in animal models and these factors may play a role in the efficacy of rehabilitation-induced recovery of cognitive and motor abilities (Murphy and Corbett, 2009; Gauthier et al., 2012). Therefore, efforts to reduce neuronal loss in combination with enhancing poststroke neural remodeling and neural plasticity provide a promising means to potentiate functional recovery. Strategies aimed at blunting the inflammatory response after stroke by depleting microglia or astrocytes have shown increased injury due to the beneficial homeostatic roles of these cells (Li et al., 2008; Szalay et al., 2016). Compared with other strategies, a unique advantage of acutely inhibiting complement amplification is that pathologic microglial and astrocyte activation is interrupted without affecting subsequent homeostatic activity required for recovery. Gene expression analysis demonstrated that CR2fH significantly downregulated several inflammatory pathways, but specifically inhibited genes involved in activation, attraction, and proliferation of immune cells and microglia on day 5, which was associated with significant reduction in microgliosis and astrocytosis at day 15. Acute administration of CR2fH also inhibited the propagation of ACP activation on day 15 after stroke, past when we would expect the inhibitor to still be present. This further supports our findings that acute complement activation initiates a self-amplification feedforward mechanism of sustained activation that is associated with persistent inflammatory and neurodegenerative changes. Acute inhibition of complement activation was not only associated with reduced inflammation and neuronal loss, but also with potentiated regenerative mechanism including increased neurogenesis and migration of neuroblasts, enhanced axonal sprouting in the perilesional brain, and enhanced synaptic density, all features

that support a favorable environment for rehabilitation and recovery. Prior work has demonstrated that complement C3a can promote increased synaptic and axonal growth after stroke if administered after 1 week of injury (Stokowska et al., 2017); however, our findings demonstrate that inhibition of complement-induced neuroinflammation acutely can disinhibit synaptic and axonal remodeling in the subacute and chronic phase. These findings emphasize the different roles that complement activation products can assume at different time windows after stroke with respect to injury versus repair and are reminiscent of proposed biphasic responses of other immune mechanisms after stroke (Lo, 2008).

The only two FDA-approved complement inhibitors, anti-C5 mAb and C1 esterase inhibitor, and nearly all complement inhibitors currently under investigation systemically inhibit complement. This is a potential problem for those at risk of infection, such as stroke patients. Complement also has various important homeostatic and physiological functions and additional concerns regarding the use of systemic complement inhibition relate to efficacy and biodistribution. An important feature of the current complement inhibition strategy is the targeting of complement inhibition to the site of complement deposition and injury, a strategy that we have shown obviates the need for systemic complement inhibition and does not affect susceptibility to infection (Atkinson et al., 2005). The construct also specifically inhibits only the ACP and permits residual complement activation driven by the classical and lectin pathway, which may contribute to immune and reparatory processes. In fact, our previous data on subacute measures after stroke demonstrated that inhibition of all complement activation pathways is not protective past the acute phase (Alawieh et al., 2015b). A humanized version of CR2fH (TT30) has been shown to be safe and nonimmunogenic in humans (Risitano et al., 2015).

In earlier studies using a rabbit model of thromboembolic stroke, data indicated that tPA activates complement because tPA administration with or without ischemic stroke reduced plasma complement hemolytic activity (Bednar et al., 1997). In a follow-up study, however, it was concluded that complement was not a primary contributor to injury in this rabbit model of stroke because complement depletion did not affect infarct size (Lew et al., 1999). More recently, Zhao et al. (2017) demonstrated that tPA administration after murine stroke induced by intraluminal filament exacerbated complement activation and increased C3a release and that C3a receptor blockade ameliorated tPA-dependent edema and hemorrhage. In this previous study, tPA was administered after reperfusion (after filament withdrawal) and motor and cognitive assessments were not made beyond 24 h of treatment.

We show here that a combination of complement inhibition by site-targeted inhibition of ACP and tPA therapy does not increase the risk of tPA-associated hemorrhage. On the contrary, combination of complement inhibition and tPA reduced tPA-associated mortality and resulted in additive effects on both motor and cognitive long-term recovery after stroke. This indicates that the mechanisms of neuroprotection engaged by tPA and CR2fH are distinct. Thrombolytic therapy reduces the extent of damage in the ischemic penumbra by restoring blood supply to the parenchyma, whereas CR2fH inhibits neuroinflammatory mechanisms that propagate damage in the ischemic penumbra. Further investigation of the interplay between complement inhibition and tPA therapy will be required to assess the pathophysiology of this interaction.

From a translational standpoint, almost every preclinical neuroprotective treatment for stroke has failed when brought to clinical trial. Potential reasons for this include: (1) treatments given too early in preclinical models, which does not translate to the clinical situation; (2) a focus on acute outcomes that do not account for chronic recovery; (3) lack of account for gender- and age-related effects; (4) a focus on gray matter injury without accounting for white matter injury; (5) no comparison of rehabilitation-induced and spontaneous recovery; and (6) lack of investigation of interaction with thrombolytic therapy. All of these points are addressed in the current study and for each we report a positive outcome after a single administration of a site-targeted inhibitor of the ACP. In addition, there is growing consensus that there is a need is for multitarget/multipathway-acting therapeutics that can selectively target injurious mechanisms and, in this context, the complement system plays a central role in inflammation and modulates multiple pathways and inflammatory mediators.

Looking forward, it will be important to better understand the detailed timeline of engagement of inflammatory and regenerative mechanisms and how delivery of complement inhibitors may alter this timeline. Such studies will help to determine the precise role of complement activation products in cerebral remodeling during long-term recovery and allow the design of an optimal approach for complement inhibitory therapy.

References

Alawieh A, Narang A, Tomlinson S (2015a) Complementing regeneration. Oncotarget 6:21769–21770. CrossRef Medline

Alawieh A, Elvington A, Zhu H, Yu J, Kindy MS, Atkinson C, Tomlinson S (2015b) Modulation of post-stroke degenerative and regenerative processes and subacute protection by site-targeted inhibition of the alternative pathway of complement. J Neuroinflammation 12:247. CrossRef Medline

Alawieh A, Wang W, Narang A, Tomlinson S (2016) Thromboembolic model of cerebral ischemia and reperfusion in mice. Methods Mol Biol 1462:357–372. CrossRef Medline

Atkinson C, Song H, Lu B, Qiao F, Burns TA, Holers VM, Tsokos GC, Tomlinson S (2005) Targeted complement inhibition by C3d recognition ameliorates tissue injury without apparent increase in susceptibility to infection. J Clin Invest 115:2444–2453. CrossRef Medline

Bednar MM, Gross CE, Russell SR, Short D, Giclas PC (1997) Activation of complement by tissue plasminogen activator, but not acute cerebral ischemia, in a rabbit model of thromboembolic stroke. J Neurosurg 86:139–142. CrossRef Medline

Brennan FH, Lee JD, Ruitenberg MJ, Woodruff TM (2016) Therapeutic targeting of complement to modify disease course and improve outcomes in neurological conditions. Semin Immunol 28:292–308. CrossRef Medline

Byblow WD, Stinear CM, Barber PA, Petoe MA, Ackerley SJ (2015) Proportional recovery after stroke depends on corticomotor integrity. Ann Neurol 78:848–859. CrossRef Medline

Carmichael ST, Kathirvelu B, Schweppe CA, Nie EH (2017) Molecular, cellular and functional events in axonal sprouting after stroke. Exp Neurol 287:384–394. CrossRef Medline

Elvington A, Atkinson C, Kulik L, Zhu H, Yu J, Kindy MS, Holers VM, Tomlinson S (2012) Pathogenic natural antibodies propagate cerebral injury following ischemic stroke in mice. J Immunol 188:1460–1468. CrossRef Medline

Falangola MF, Guilfoyle DN, Tabesh A, Hui ES, Nie X, Jensen JH, Gerum SV, Hu C, LaFrancois J, Collins HR, Helpern JA (2014) Histological correlation of diffusional kurtosis and white matter modeling metrics in cuprizone-induced corpus callosum demyelination. NMR Biomed 27:948–957. CrossRef Medline

Gauthier LV, Taub E, Mark VW, Barghi A, Uswatte G (2012) Atrophy of spared gray matter tissue predicts poorer motor recovery and rehabilitation response in chronic stroke. Stroke 43:453–457. CrossRef Medline

Geiss GK, Bumgarner RE, Birditt B, Dahl T, Dowidar N, Dunaway DL, Fell HP, Ferree S, George RD, Grogan T, James JJ, Maysuria M, Mitton JD, Oliveri P, Osborn JL, Peng T, Ratcliffe AL, Webster PJ, Davidson EH,

Hood L (2008) Direct multiplexed measurement of gene expression with color-coded probe pairs. Nat Biotechnol 26:317–325. CrossRef Medline

Huang J, Kim LJ, Mealey R, Marsh HC Jr, Zhang Y, Tenner AJ, Connolly ES Jr, Pinsky DJ (1999) Neuronal protection in stroke by an sLex-glycosylated complement inhibitory protein. Science 285:595–599. CrossRef Medline

Huang Y, Qiao F, Atkinson C, Holers VM, Tomlinson S (2008) A novel targeted inhibitor of the alternative pathway of complement and its therapeutic application in ischemia/reperfusion injury. J Immunol 181:8068–8076. CrossRef Medline

Hui ES, Fieremans E, Jensen JH, Tabesh A, Feng W, Bonilha L, Spampinato MV, Adams R, Helpern JA (2012) Stroke assessment with diffusional kurtosis imaging. Stroke 43:2968–2973. CrossRef Medline

Jones TA, Adkins DL (2015) Motor system reorganization after stroke: stimulating and training toward perfection. Physiology (Bethesda) 30:358–370. CrossRef Medline

Lew SM, Gross CE, Bednar MM, Russell SJ, Fuller SP, Ellenberger CL, Howard D (1999) Complement depletion does not reduce brain injury in a rabbit model of thromboembolic stroke. Brain Res Bull 48:325–331. CrossRef Medline

Li L, Lundkvist A, Andersson D, Wilhelmsson U, Nagai N, Pardo AC, Nodin C, Ståhlberg A, Aprico K, Larsson K, Yabe T, Moons L, Fotheringham A, Davies I, Carmeliet P, Schwartz JP, Pekna M, Kubista M, Blomstrand F, Maragakis N (2008) Protective role of reactive astrocytes in brain ischemia. J Cereb Blood Flow Metab 28:468–481. CrossRef Medline

Lo EH (2008) A new penumbra: transitioning from injury into repair after stroke. Nat Med 14:497–500. CrossRef Medline

Mi H, Poudel S, Muruganujan A, Casagrande JT, Thomas PD (2016) PANTHER version 10: expanded protein families and functions, and analysis tools. Nucleic Acids Res 44:D336–D342. CrossRef Medline

Mocco J, Mack WJ, Ducruet AF, Sosunov SA, Sughrue ME, Hassid BG, Nair MN, Laufer I, Komotar RJ, Claire M, Holland H, Pinsky DJ, Connolly ES Jr (2006) Complement component C3 mediates inflammatory injury following focal cerebral ischemia. Circ Res 99:209–217. CrossRef Medline

Moran J, Stokowska A, Walker FR, Mallard C, Hagberg H, Pekna M (2017) Intranasal C3a treatment ameliorates cognitive impairment in a mouse model of neonatal hypoxic-ischemic brain injury. Exp Neurol 290:74–84. CrossRef Medline

Murphy TH, Corbett D (2009) Plasticity during stroke recovery: from synapse to behaviour. Nat Rev Neurosci 10:861–872. CrossRef Medline

Patil SS, Sunyer B, Höger H, Lubec G (2009) Evaluation of spatial memory of C57BL/6J and CD1 mice in the barnes maze, the multiple T-maze and in the morris water maze. Behav Brain Res 198:58–68. CrossRef Medline

Pekna M, Pekny M, Nilsson M (2012) Modulation of neural plasticity as a basis for stroke rehabilitation. Stroke 43:2819–2828. CrossRef Medline

Risitano AM, Storek M, Sahelijo L, Doyle M, Dai Y, Weitz IC, Marsh JCW, Elebute M, O'Connell CL, Kulasekararaj AG, Ramsingh G, Marotta S, Hellmann A, Lundberg AS (2015) Safety and pharmacokinetics of the complement inhibitor TT30 in a phase I trial for untreated PNH patients. Blood 126:2137.

Ruscher K, Kuric E, Liu Y, Walter HL, Issazadeh-Navikas S, Englund E, Wieloch T (2013) Inhibition of CXCL12 signaling attenuates the postischemic immune response and improves functional recovery after stroke. J Cereb Blood Flow Metab 33:1225–1234. CrossRef Medline

Stokowska A, Atkins AL, Moran J, Pekny T, Bulmer L, Pascoe MC, Barnum SR, Wetsel RA, Nilsson JA, Dragunow M, Pekna M (2017) Complement peptide C3a stimulates neural plasticity after experimental brain ischaemia. Brain 140:353–369. CrossRef Medline

Szalay G, Martinecz B, Lénárt N, Környei Z, Orsolits B, Judák L, Császár E, Fekete R, West BL, Katona G, Rózsa B, Dénes Á (2016) Microglia protect against brain injury and their selective elimination dysregulates neuronal network activity after stroke. Nat Commun 7:11499. CrossRef Medline

Tabesh A, Jensen JH, Ardekani BA, Helpern JA (2011) Estimation of tensors and tensor-derived measures in diffusional kurtosis imaging. Magn Reson Med 65:823–836. CrossRef Medline

Tennant KA, Asay AL, Allred RP, Ozburn AR, Kleim JA, Jones TA (2010) The vermicelli and capellini handling tests: simple quantitative measures of dexterous forepaw function in rats and mice. J Vis Exp 41:2076. CrossRef Medline

Tennant KA, Kerr AL, Adkins DL, Donlan N, Thomas N, Kleim JA, Jones TA (2015) Age-dependent reorganization of peri-infarct "premotor" cortex with task-specific rehabilitative training in mice. Neurorehabil Neural Repair 29:193–202. CrossRef Medline

Türeyen K, Vemuganti R, Sailor KA, Dempsey RJ (2004) Infarct volume quantification in mouse focal cerebral ischemia: a comparison of triphenyltetrazolium chloride and cresyl violet staining techniques. J Neurosci Methods 139:203–207. CrossRef Medline

Umesh Rudrapatna S, Wieloch T, Beirup K, Ruscher K, Mol W, Yanev P, Leemans A, van der Toorn A, Dijkhuizen RM (2014) Can diffusion kurtosis imaging improve the sensitivity and specificity of detecting microstructural alterations in brain tissue chronically after experimental stroke? Comparisons with diffusion tensor imaging and histology. Neuroimage 97:363–373. CrossRef Medline

Weber RA, Hui ES, Jensen JH, Nie X, Falangola MF, Helpern JA, Adkins DL (2015) Diffusional kurtosis and diffusion tensor imaging reveal different time-sensitive stroke-induced microstructural changes. Stroke 46:545–550. CrossRef Medline

Xiong B, Li A, Lou Y, Chen S, Long B, Peng J, Yang Z, Xu T, Yang X, Li X, Jiang T, Luo Q, Gong H (2017) Precise cerebral vascular atlas in stereotaxic coordinates of whole mouse brain. Front Neuroanat 11:128. CrossRef Medline

Yu K, Wu Y, Hu Y, Zhang Q, Xie H, Liu G, Chen Y, Guo Z, Jia J (2013) Neuroprotective effects of prior exposure to enriched environment on cerebral ischemia/reperfusion injury in rats: the possible molecular mechanism. Brain Res 1538:93–103. CrossRef Medline

Zhang L, Schallert T, Zhang ZG, Jiang Q, Arniego P, Li Q, Lu M, Chopp M (2002) A test for detecting long-term sensorimotor dysfunction in the mouse after focal cerebral ischemia. J Neurosci Methods 117:207–214. CrossRef Medline

Zhao XJ, Larkin TM, Lauver MA, Ahmad S, Ducruet AF (2017) Tissue plasminogen activator mediates deleterious complement cascade activation in stroke. PLoS One 12:e0180822. CrossRef Medline

Zhuo J, Xu S, Proctor JL, Mullins RJ, Simon JZ, Fiskum G, Gullapalli RP (2012) Diffusion kurtosis as an in vivo imaging marker for reactive astrogliosis in traumatic brain injury. Neuroimage 59:467–477. CrossRef Medline